AD-A136 071 PHASE CONJUGATE OPTICAL RESONATOR(U) HUGHES RESEARCH LAB MALIBU CA R A MCFARLANE ET AL. NOV 83 AFOSR-TR-83-1093 F49620-80-C-0041 1/1

UNCLASSIFIED F/G 20/6 NL

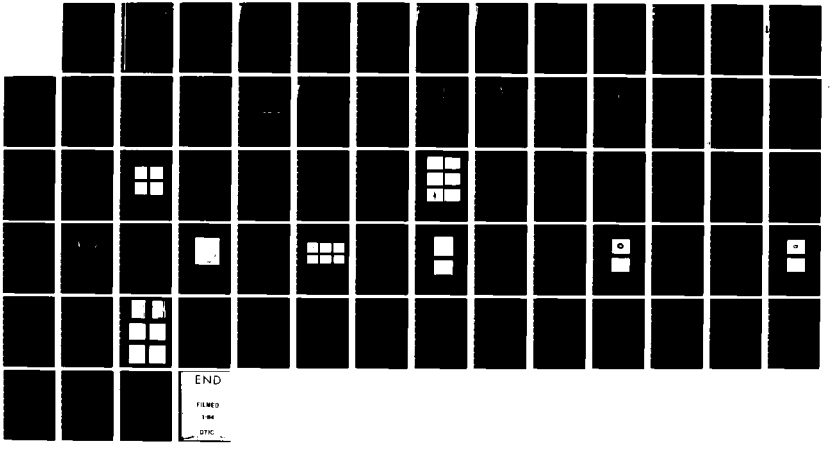

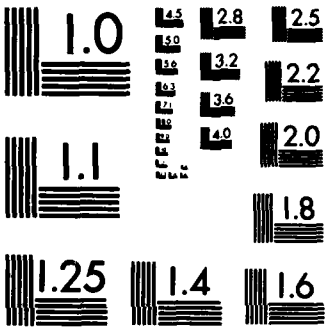

PHASE CONJUGATE OPTICAL RESONATOR

R.A. McFarlane, R.C. Lind, G.J. Dunning, R.K. Jain,
J.F. Lam, D.G. Steel, and G.C. Valley

Hughes Research Laboratories
3011 Malibu Canyon Road
Malibu, CA 90265

November 1983

F49620-80-C-0041
Final Report
15 January 1980 through 14 April 1983

AIR FORCE OFFICE OF SCIENTIFIC RESEARCH
Bolling AFB, DC 20332

UNCLASSIFIED

SECURITY CLASSIFICATION OF THIS PAGE *(When Data Entered)*

REPORT DOCUMENTATION PAGE	READ INSTRUCTIONS BEFORE COMPLETING FORM
1. REPORT NUMBER **AFOSR-TR- 83-1093** 2. GOVT ACCESSION NO. AD-A136071	3. RECIPIENT'S CATALOG NUMBER
4. TITLE *(and Subtitle)* Phase Conjugate Optical Resonator	5. TYPE OF REPORT & PERIOD COVERED Final Report 15 Jan. 1980 - 14 Apr. 1983 6. PERFORMING ORG. REPORT NUMBER
7. AUTHOR(s) R.A. McFarlane, R.C. Lind, G.J. Dunning, R.K. Jain, J.F. Lam, D.G. Steel and G.C. Valley	8. CONTRACT OR GRANT NUMBER(s) F49620-80-C-0041
9. PERFORMING ORGANIZATION NAME AND ADDRESS Hughes Research Laboratories 3011 Malibu Canyon Road Malibu, CA 90265	10. PROGRAM ELEMENT, PROJECT, TASK AREA & WORK UNIT NUMBERS 61102F 2301/A1
11. CONTROLLING OFFICE NAME AND ADDRESS Air Force Office of Scientific Research Bolling AFB, DC 20332	12. REPORT DATE November 1983 13. NUMBER OF PAGES 75
14. MONITORING AGENCY NAME & ADDRESS*(if different from Controlling Office)*	15. SECURITY CLASS. *(of this report)* UNCLASSIFIED 15a. DECLASSIFICATION/DOWNGRADING SCHEDULE

16. DISTRIBUTION STATEMENT *(of this Report)*

Approved for public release; distribution unlimited.

17. DISTRIBUTION STATEMENT *(of the abstract entered in Block 20, if different from Report)*

18. SUPPLEMENTARY NOTES

19. KEY WORDS *(Continue on reverse side if necessary and identify by block number)*

Phase conjugation, Laser resonators, Optical resonators, Degenerate four-wave mixing, Phase conjugate mirror, Laser modes, Aberration correction, Self-pumped phase conjugate mirror, Photorefractive, $BaTiO_3$.

→ This is the the properties of conjugate resonator.

20. ABSTRACT *(Continue on reverse side if necessary and identify by block number)*

Final report on a program to study phase conjugate optical resonators. Laser oscillation was achieved using both atomic sodium and photorefractive $BaTiO_3$ in four-wave mixing geometry as a phase ~~conjugator~~. Spectral and transverse mode characteristics were measured. A self-pumped phase conjugate mirror was also used in an oscillator and a computer code developed to model power output and transverse mode profile. Aberration correction was demonstrated.

DD FORM 1 JAN 73 1473 EDITION OF 1 NOV 65 IS OBSOLETE

UNCLASSIFIED

SECURITY CLASSIFICATION OF THIS PAGE *(When Data Entered)*

TABLE OF CONTENTS

LIST OF ILLUSTRATIONS

FOREWORD

This report was prepared by Hughes Research Laboratories (HRL) under Contract No. F49620-80-C-0041. It describes work performed from January 15, 1980 to April 1, 1983. The principal investigator during the first half of the program was R.C. Lind; during the latter half the principle investigator was R.A. McFarlane. The experimental effort during this period was carried out by G.J. Dunning, R.K. Jain, R.C. Lind, R.A. McFarlane, and D.G. Steel. J.F. Lam and G.C. Valley participated in the theoretical analysis of phase conjugate mirrors and laser performance. J.E. Brown and J.P. Shuler contributed technical assistance in the laboratory.

ACKNOWLEDGMENT

The authors wish to thank R.L. Abrams of the Space and Communications Group, and C.R. Giuliano, manager of the Optical Physics Department, for their technical advice and support during the program. We also wish to thank B. Feldman and H.R. Schlossberg of AFOSR for their interest in and support of this work.

SECTION 1

PHASE CONJUGATE RESONATOR

This is the final technical report in a program to study the properties of phase conjugate optical resonators. In particular, the objectives of the program were to demonstrate oscillation in a phase conjugate resonator (PCR), to examine its mode properties, compare experiment with theory where possible, and finally, to simplify PCR operation by employing as the pump source for the conjugating element, some of the output power of the laser itself. We believe the program has achieved these objectives.

The unique property of phase conjugate mirrors to generate so-called time-reversed wavefronts has been demonstrated by workers at HRL and elsewhere. The use of this phenomenon to compensate for optical aberrations makes it a promising candidate for intracavity application.

The multipass character of laser oscillators greatly enhances the distortion potential of intracavity perturbations. In particular, the effect of laser medium index inhomogeneities resulting from flow variations, pump variations, or simply thermal effects can degrade the wavefront exiting from a laser to a larger extent than can a similar extracavity disturbance. Similarly, the effect of mirror misalignments is greatly accentuated as compared to normal (extracavity) optical trains.

In principle, the resulting wavefront errors can be corrected either intracavity or extracavity. However, these internal errors lead to both amplitude distortions and vignetting of the output beams that are not easily compensated with extracavity systems. Further, the resulting intracavity errors may sometimes have a very high spatial frequency content. Since nonlinear conjugation and/or other nonlinear compensation offers excellent capability for correcting high spatial frequency distortion, as contrasted with conventional adaptive

optics with deformable mirrors, it provides an important motivation for using such systems in intracavity compensation. In addition, a conjugate resonator offers the promise of recovering some of the energy that would be lost by diffraction in an ordinary resonator, resulting in improved energy extraction from the gain medium. Finally, the nonlinear approaches offer the ultimate promise of simplicity and low cost compared with deformable mirror systems.

Yet despite the potential just discussed, there are many open questions concerning the application of nonlinear compensation in laser oscillators; the work performed on this program was aimed at answering some of these questions.

SECTION 2

PROGRAM ACCOMPLISHMENTS

During the first year and a half of this AFOSR program we reported three significant accomplishments: (1) the first experimental demonstration of phase conjugate reflectivities higher than unity in a cw phase conjugate mirror (PCM) possessing a large dynamic bandwidth, (2) a detailed study on pump-probe detuning effects in this PCM, and on the basis of these studies, (3) demonstration of a cw phase conjugate resonator (PCR) employing a cw dye amplifier as the gain medium. These experiments demonstrated the longitudinal modes and aberration correction properties of a PCR, which differ significantly from that of a conventional laser.

In the next year of the program we carried out detailed studies of the spatial and temporal properties of a cw PCR employing a photorefractive crystal, $BaTiO_3$. In the final period we demonstrated the operation of a particularly simple laser oscillator using a self-pumped phase conjugate mirror configuration. Studies of the spectral properties, aberration correction and a computer modeling of this self-pumped PCR are reported here for the first time.

A. HIGH-REFLECTIVITY LARGE-BANDWIDTH PCM

Phase conjugate optical resonators[1-5] require the use of one or more phase conjugate mirrors. Our studies concentrated on a linear resonator employing one PCM and a conventional mirror. The constraints imposed on the design specifications of the PCM clearly depend on the performance characteristics expected from the PCR. Aside from the study of very interesting and highly unique behavior in their longitudinal and transverse mode properties,[4,7] PCRs are expected to find application in laser systems characterized by highly aberrating turbulence.

Given the dynamic behavior of turbulence, this application requires real-time aberration correction. Therefore, the PCM used in such a phase conjugate resonator needs to be characterized by a response time shorter than the characteristic time of turbulence. Thus, our experimental studies on a high reflectivity PCM focused on the use of a material with a relatively high response speed. This was obtained with the use of sodium vapor, whose response time is typically on the order of nanoseconds. Also, in order to allow sufficient time for the buildup of the modes, and for a clean and detailed study of the same, we emphasized the development of high reflectivities under cw operation rather than pulsed operation.

Due to limitations on the net gain that may be obtained easily with cw amplifiers, it was necessary that the PCM reflectivities be of the order of 40% or higher. Reflectivities exceeding unity, and typically on the order of 80%, were demonstrated using the configuration of Figure 1. In this configuration, the counterpropagating pump is obtained by splitting the main beam into a forward and backward pump. It is important to operate with separate pumps to avoid the unbalanced pump powers occurring in the more standard technique of passing the forward pump through the conjugator and then retro-reflecting this beam backward to generate the backwqard pump. The unbalanced pumps resulting from the latter configuration produce a decrease in the reflectivity due to a reduction in the nonlinear response. This effect is a characteristic of the saturating resonant linearity, such as that encountered in Na vapor.

For our experiments, the pump beams were obtained from a Coherent Radiation 699-21 stabilized dye laser which produced 1.2 W of single line power. These beams were focused with a 1 m focal length lens into the Na cell which was a simple 1-cm-long side-arm cell. To achieve high reflectivities, the sodium pressure was adjusted near 10^{-3} Torr; the high cw output of the dye laser resulted in only nominal absorption in the Na vapor.

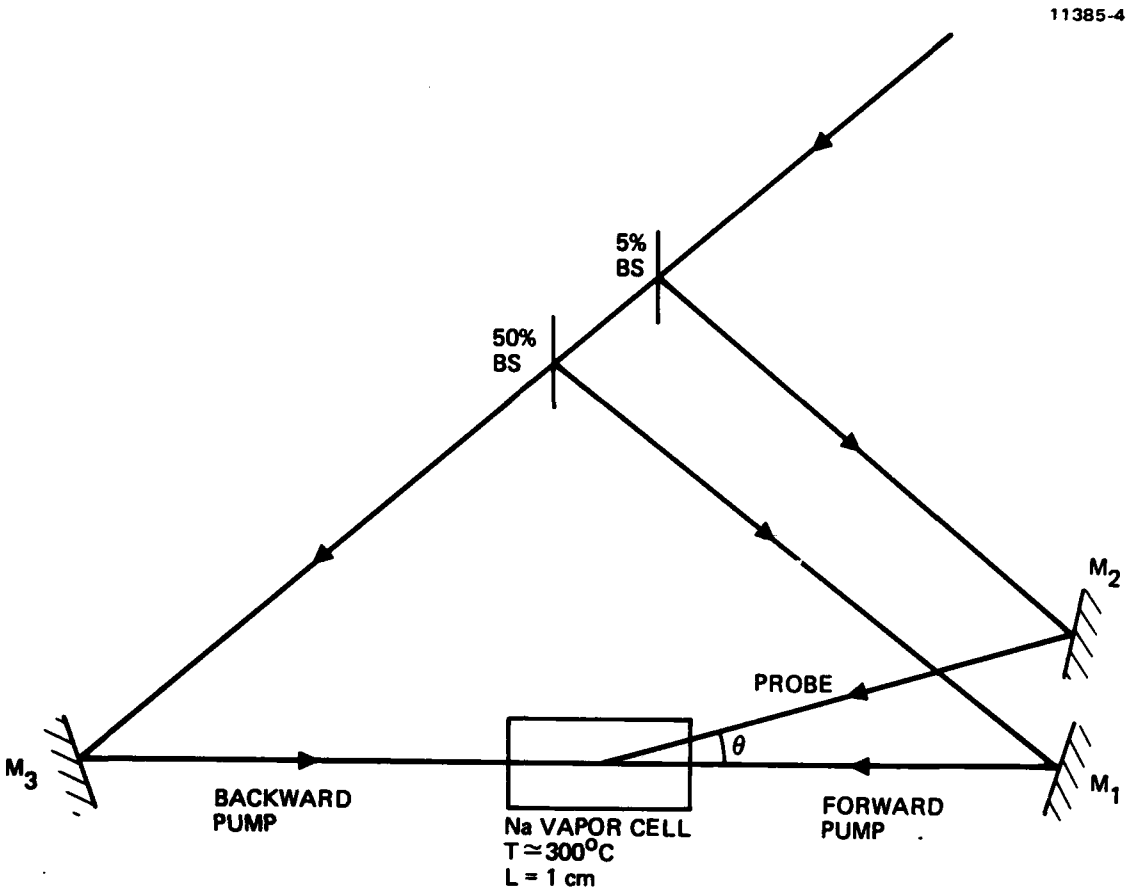

Figure 1. Experimental configuration for measurements of high efficiency DFWM. Reflectivities in excess of 150% were measured in atomic sodium.

In addition to these factors, the linearly polarized pumps necessitated the maintenance of a very small angle ($\theta < 0.5°$) between the forward pump and the probe to maximize the reflectivity, where the probe path is the path over which the PCR will oscillate. This sensitivity to angle is shown in the paper of Nilsen and Yariv[8] and is a characteristic of an inhomogeneously broadened medium such as Na vapor.

It is important to note that the high reflectivities are only achieved by appropriately detuning the laser off line-center of the D_2 transition, and by operation of the pump laser

in a single longitudinal mode. The dependence of the reflectivity on the pump frequency (assuming degenerate operation) is quite complex due to the hyperfine splitting of the D_2 line (λ = 589 nm) into 6 dipole-allowed transitions. Optical pumping and the presence of many crossover resonances adds to the difficulty. Nevertheless, detailed studies of the PCM using the 699-21 dye laser have resulted in a fairly complete understanding of the various processes. While earlier work[6] on DFWM in Na vapor indicated that the largest reflectivity (R ~ 0.22%) was observed on the $3s^2S_{1/2}$ (F = 2) - $3p^2P_{3/2}$ (F = 3) h.f. transition, these new experiments showed that the largest reflectivities (R ~ 150%) occurred near the $3s^2S_{1/2}$ (F = 1) - $3p^2P_{3/2}$ (F = 0) transition.

B. PUMP-PROBE DETUNING CHARACTERISTICS: NEARLY-DEGENERATE FWM IN SODIUM VAPOR

One of the key features that distinguishes a conventional laser resonator from a PCR is the longitudinal mode structure observed in the output frequency spectrum of the PCR. While modes of an ordinary laser resonator are spaced by c/2L, the modes of the resonator incorporating a phase conjugate mirror are spaced by approximately c/4L and occur in pairs symmetrically spaced about the central frequency.[2] The central frequency always corresponds to the pump frequency of the PCM and is not dependent on the cavity length.

The longitudinal mode properties of the PCR are related to nearly-degenerate four-wave mixing in the nonlinear material comprising the PCM. In order to understand these longitudinal mode properties, it is necessary to examine the pump-probe detuning characteristics for nearly-degenerate four-wave mixing (FWM) in sodium vapor. These pump-probe detuning characteristics can be quite complicated in Na vapor due to the occurrence of multiresonant behavior and the ac Stark effect; we have studied this experimentally at both low and high light

intensities. A report on this material has been published in Optics Letters.[9]

The experimental study of nearly degenerate four-wave mixing was performed using the experimental configuration shown in Figure 2. The laser sources for the pumps ($\omega_f = \omega_b \equiv \omega_1$) and probe ($\omega_p = \omega_2$) were two stabilized Coherent 699-21 tunable dye lasers with linewidths on the order of 1 MHz. The resonant atomic medium was sodium and the lasers were tuned near the D_2 line (5890 Å). Due to the half-integral spin of the Na nucleus, the spectroscopy of the D_2 line is quite complex, with six allowed dipole transitions. Optical pumping plays an important role in the precise interpretation of any experiment involving sodium. However, when linear polarized light is used the effects are minimized by working on the strongest dipole transition, viz., the $3s^2S_{1/2}$ (F = 2) - $3p^2P_{3/2}$ (F = 3) transition, characterized by a saturation intensity on the order

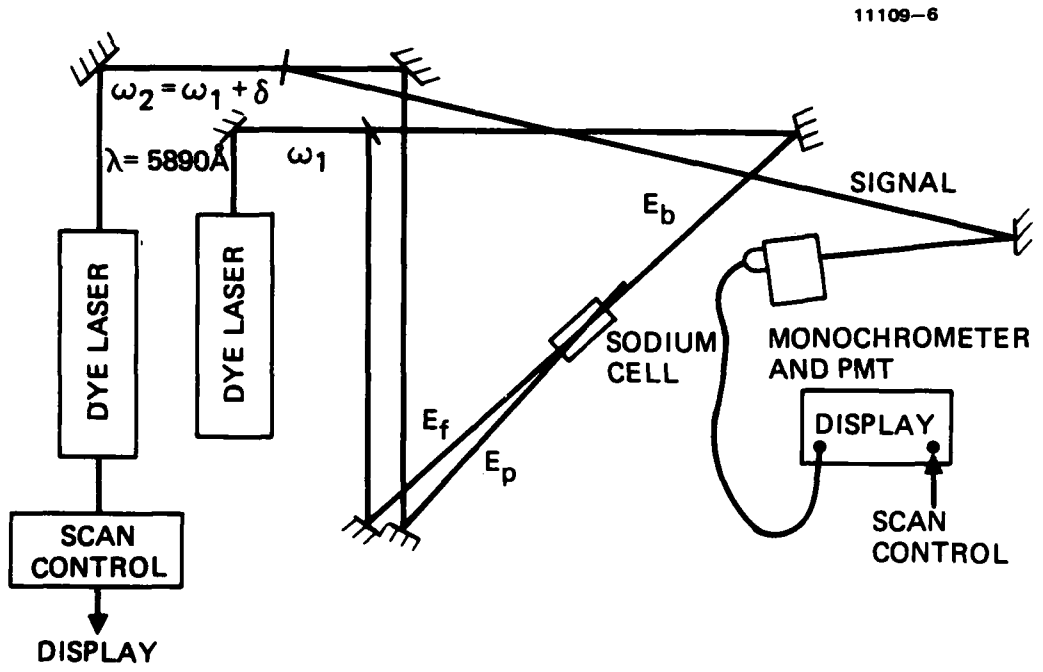

Figure 2. Experimental layout for studying nearly-degenerate FWM.

of 6 mW/cm^2. For these experiments, the angle between the pump and probe was again kept small to maximize the signal-to-probe reflectivity. In all cases the probe intensity was kept well below the pump intensity. The absorption length product ($\alpha_o \ell$) was kept at the order of unity.

Let us first consider a general feature of nearly degenerate FWM, which stems from energy conservation ($\omega_f + \omega_b - \omega_p - \omega_s = 0$) and phase matching ($\bar{k}_f + \bar{k}_b - \bar{k}_p - \bar{k}_s = 0$). If the two pumps ($\omega_f$, ω_b) are tuned at ω_1, and the probe is tuned to $\omega_p \equiv \omega_2 = \omega_1 + \delta$, such that $\delta << \omega_1$, it follows that a counterpropagating ($\bar{k}_s = -\bar{k}_p$) signal wave is generated at $\omega_s = \omega_1 - \delta$, as shown in Figure 3. This general feature is applicable for all nearly-degenerate FWM experiments and is independent of the energy level structure of the nonlinear medium.

Our first measurements were on the experimental verification of such behavior, since it is the physical basis for the occurrence of the paired half-axial modes predicted for PCRs. Figure 4 shows a scanning Fabry-Perot trace of the signal when the probe is detuned from the pumps. (The figure also shows the probe frequency.) As expected, the signal was displaced from the pump frequency by an amount, $-\delta$, when the probe was detuned an amount, $+\delta$, from the pump. No additional structure was observed at either low or high pump intensities.

The second general problem we confronted, and one that is very relevant to the understanding of the PCR, especially in light of the effective bandwidth of the PCM, was the analysis of pump-probe detuning in a Doppler-broadened medium for both low ($I << I_{sat}$) and high ($I >> I_{sat}$) intensities.[8,10] The Doppler-broadened problem had been solved earlier using third-order perturbation theory in the limit of low intensity pumps. For a given pump detuning from resonance $\Delta(\omega_1 = \omega_o + \Delta)$, it is possible to determine the resonance condition for the

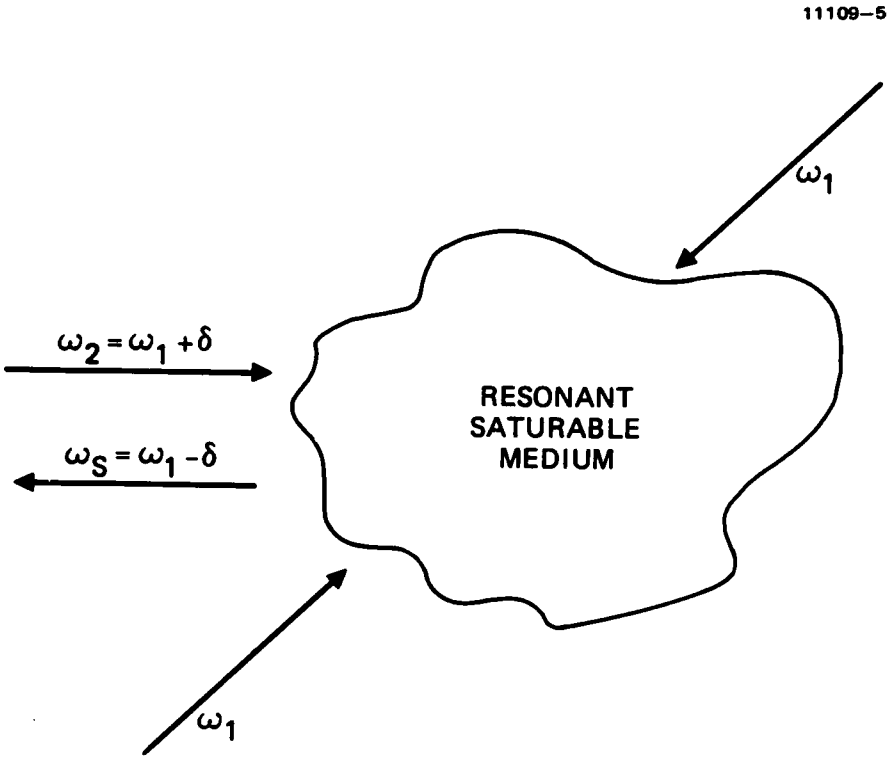

Figure 3. Geometry for nearly-degenerate FWM. The pumps are at frequency, ω_1, but the probe is shifted by an amount, δ.

pump-probe detuning, δ. The resonances are given by $\delta = 0$ ($\omega_2 = \omega_o + \Delta$) and $\delta = 2\Delta$ ($\omega_2 = \omega_o + 3\Delta$). The first resonance occurs when the detuning between the two beams is less than the linewidth, enabling both the forward pump and probe to interact simultaneously with the same group of atoms and to produce a spatial modulation of the population from which the backward pump can scatter. The physical origin of the second resonance is somewhat more subtle, arising from a combination of Doppler effects. The forward pump at ω_1, detuned from the resonance frequency, ω_o, by Δ, is Doppler-shifted into resonance for a particular velocity group, v. The resonance observed in tuning the probe to $\delta = 2\Delta$ occurs at a frequency when the atom (in the rest frame) sees the Doppler-shifted probe and backward pump at the same frequency.

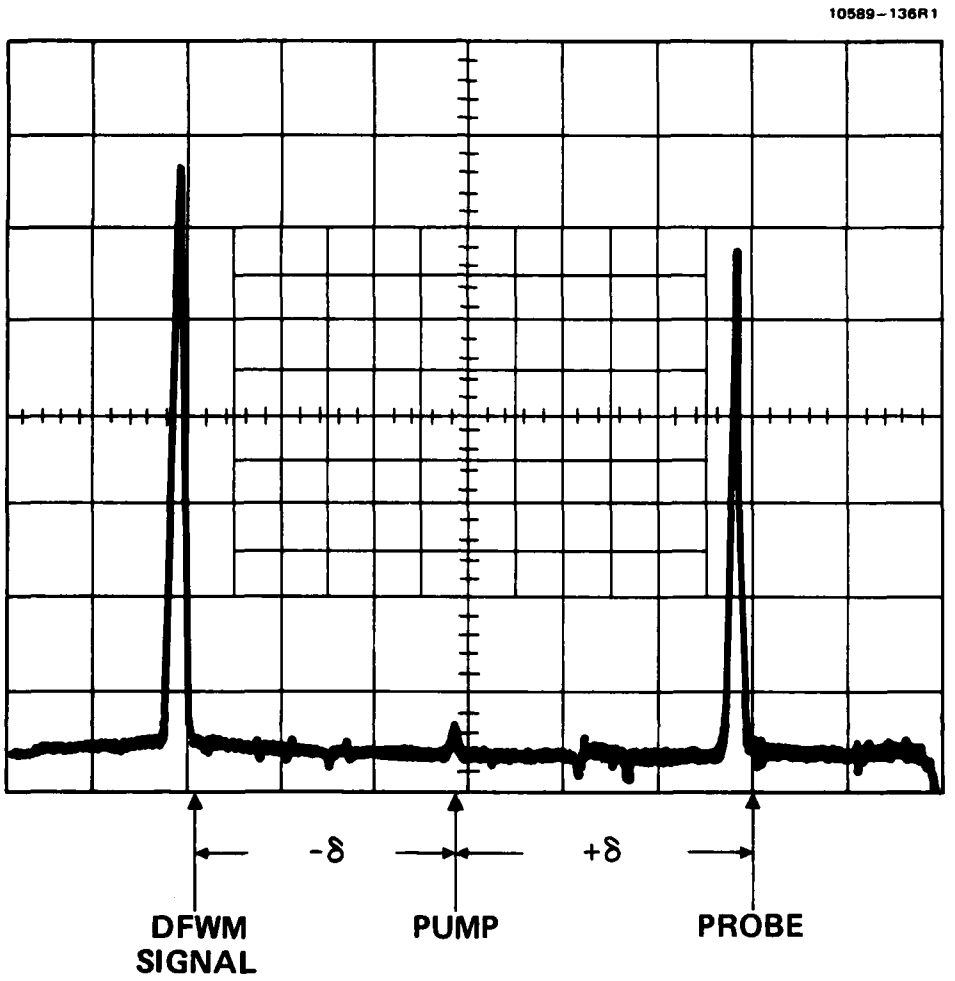

Figure 4. Scanning Fabry-Perot picture showing the frequency shift of the signal wave ($-\delta$) with respect to the frequency shift of the input probe (δ), demonstrating that because of phase matching, $\omega_1 + \omega_1 - \omega_2 - \omega_s = 0$.

The pump-probe detuning problem has also been examined in the presence of arbitrarily strong pump fields in homogeneously broadened Doppler-free media. A steady-state solution to the quantum mechanical transport equation was found, which was valid to all orders in the pump field and to first order in the probe and signal.[11,12] The qualitative solution to this problem may be anticipated by recalling the behavior of a two-level atom subject to a strong field at frequency, ω_1, and tuned near resonance at ω_o. The population will undergo strong oscillation between the two levels at an angular frequency, given by the generalized Rabi frequency, $\Omega' = [(\omega_1 - \omega_o)^2 + \Omega^2]^{1/2}$, where $\Omega = \mu E/h$ is the transition dipole and E is the electric field. This effect can be viewed as a splitting of each level into two levels separated by an energy, $h\,\Omega'$, and is known as the A.C. Stark effect. Hence, one would expect such a system to be characterized by three resonances at frequencies $\delta = 0$ and $\delta = \pm\Omega'$. However, in nearly degenerate FWM the presence of strong counter propagating pumps complicates this expectation. The simultaneous action of both pumps produces a standing wave modulation of the net electric field. Hence, the Stark splitting of the levels is also spatially modulated, producing a macroscopic polarization, with resonances anticipated by the presence of high intensity fields and low intensity fields. Using perturbation theory in Doppler-free media, one can show that in the presence of low intensity pumps, pump probe detuning resonances occur at $\delta = 0$ and $\delta = \pm\Delta$. Hence, a total of five resonances are expected.[12] The ability to observe the low intensity resonances in Doppler-broadened media would only be expected if the power broadening exceeded the pump detuning, Δ.

The experimentally measured dependence of reflectivity as a function of pump-probe detuning (δ) was taken at low pump intensity ($I < I_{SAT}$) for various pump detunings from the atomic resonance (Δ). Figure 5 shows the evolution of the resonant structure for various Δ as a function of probe frequency. As

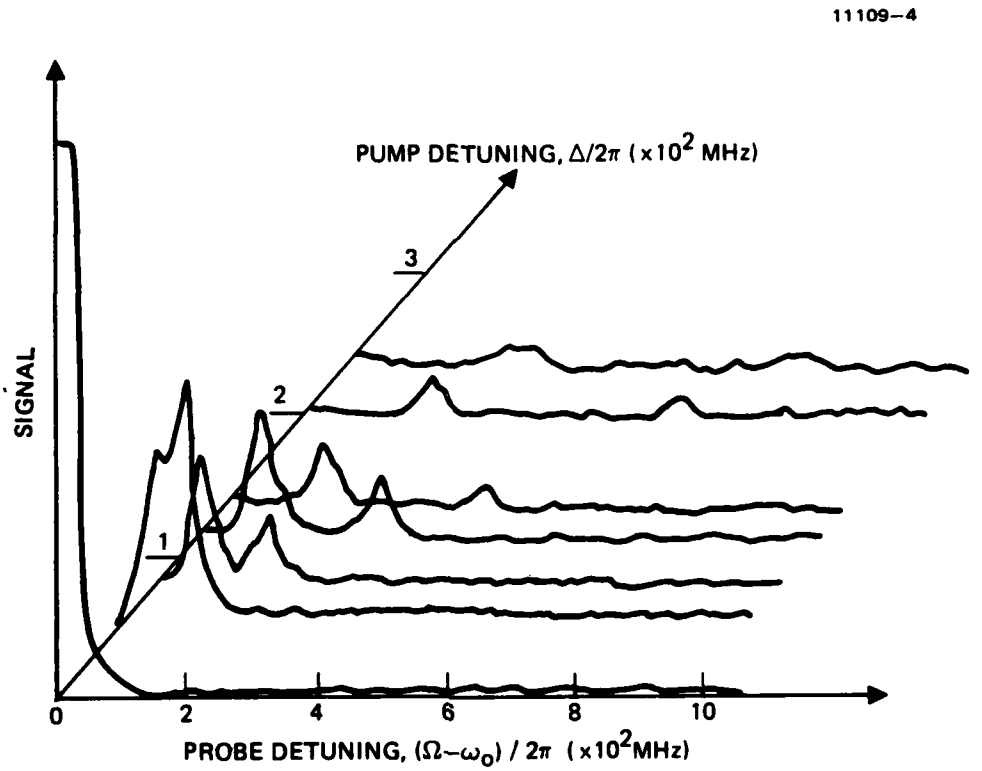

Figure 5. Experimental demonstration of multiresonant behavior of nearly degenerate FWM for low pump intensity. The frequency shifts occur at $\omega = \Delta$ and $\delta = 2\Delta$ as expected for inhomogeneously broadened material.

anticipated above, when $\Delta = 0$, there is a strong, single resonance. However, as Δ is increased, two resonances form at $\delta = \Delta$ and $\delta = 2\Delta$. The bandwidth of the central resonance is determined by the longitudinal relaxation rate. For a two-level problem, with the lower state being the ground state, that rate is given by the A-coefficient. Hence the bandwidth is twice as large as the atomic linewidth. Physically, this rate is determined by how fast the population (rather than the induced optical coherence) can respond to the time-dependent optical field oscillating at $\omega_2 - \omega_1$ (in the rotating wave approximation). Figure 6 shows the measured bandwidth with

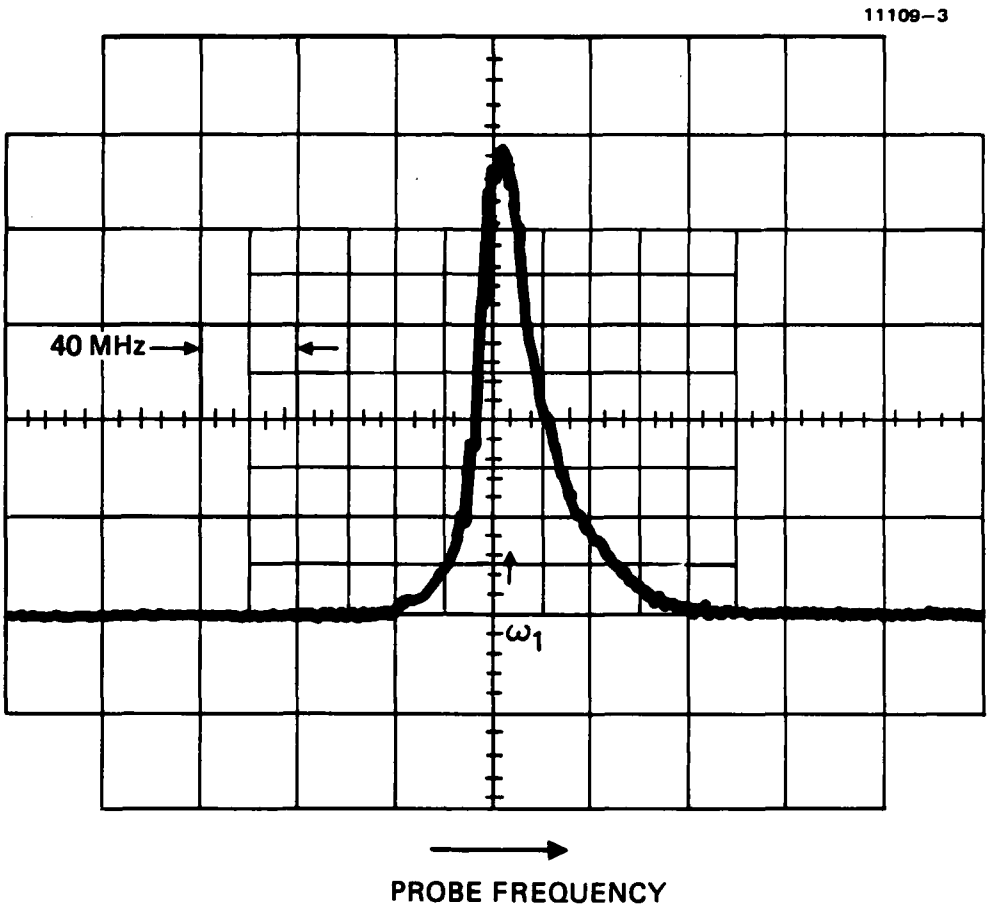

Figure 6. The measured bandwidth of the pump-probe detuning response at low pump intensity. The width is determined by the longitudinal relaxation rate, T_1^{-1}.

$\Delta = 0$. The measured bandwidth is 25 MHz in good agreement with the expected value of 20 MHz.

As expected at high intensities, the pump detuning dependence is considerably more complicated. The interaction is further complicated in sodium by atomic motion and hyperfine structure. Nevertheless, by appropriate choices for the pump detuning, Δ, and pump intensity, I, it was possible to qualitatively verify the above predictions of multiresonant behavior. Shown in Figure 7 is the observed five-peak behavior predicted by Harter and Boyd.[12] The pump detuning was $\Delta = 210$ MHz, giving a generalized Rabi frequency of $\Omega' = 421$ MHz. As the figure

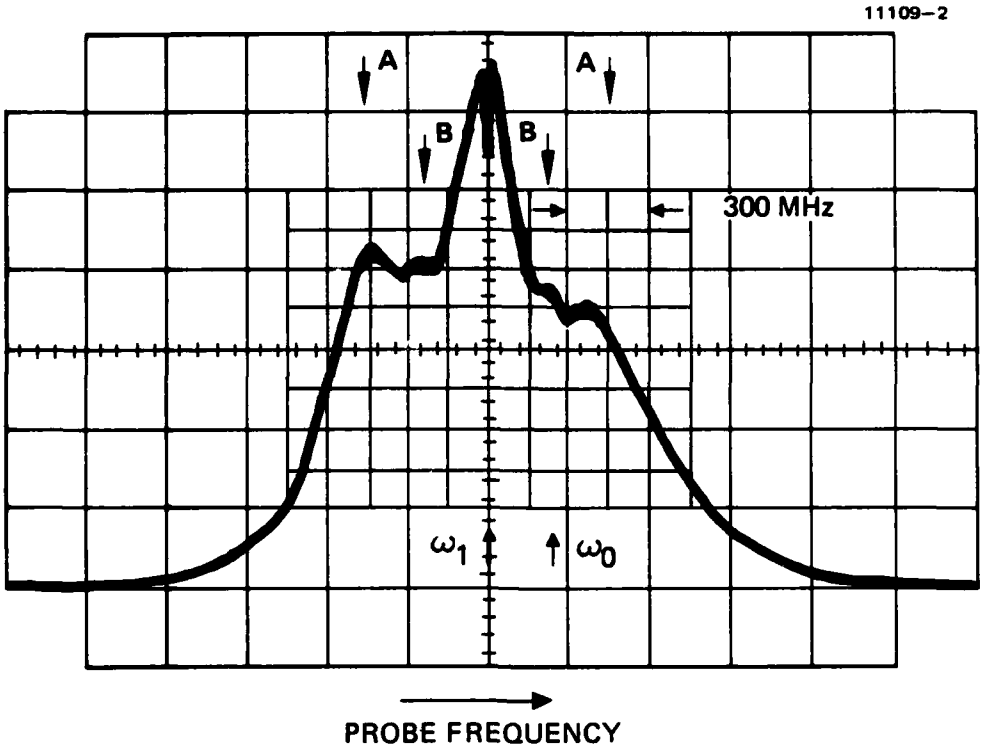

Figure 7. The pump-probe detuning response as measured at high pump intensity. Five resonances are observed. The central resonance occurs at $\delta = 0$. The two structures designated B occur at $\delta = \pm\Delta$. The two structures designated A are due to the ac Stark splitting of the atomic levels and occur at $\delta = \pm\Omega$.

shows, the location of the sidebands (structure A) agrees excellently with Ω'. Structure B is the resonance occurring at $\delta = \pm\Delta$ on the pump electric field and is expected to be complicated due to velocity effects in the prescence of an electric-field standing wave. However, our measurements show that over a range of $0.1 < E < 0.45$ sV/cm the measured Ω' corresponds to the calculated value.

Not easily predicted or understood is the dip occuring at $\delta = 0$. This structure has been observed to to be very narrow

(~ 30 MHz). Sucn an effect has been predicted to arise between the probe and signal at $\delta \neq 0$. Such an explanation is not easily adapted to our data since this microstructure is a dip for $\Delta < 0$ and a spike for $\Delta > 0$ on the $3s^2S_{1/2}$ (F - 2) $-3p^2P_{3/2}$ (F - 3) transition. Further, for transitions out of the F = 1 ground state, it is a dip for $\Delta > 0$ and a spike for $\Delta < 0$. Additional studies are in progress.

The net bandwidth in Figure 7 is given by 2 Ω'. However, as the absorption length product is increased, the bandwidth is observed to narrow significantly and secondary resonances are not observed. This is because the probe and signal are strongly absorbed as the detuning, δ, exceeds the frequency width of the hole burned by the strong saturating pumps. Furthermore, at high $\alpha_o \ell$, the phase matching is no longer perfect, due to a finite dispersion. Additional narrowing is also expected at high R, due to so-called feedback narrowing. However, under these conditions the reflectivity is over 150% on the $3s^2S_{1/2}$ (F = 1) $-3p^2{}_{3/2}$ (F = 0) transitions. An example of such a bandwidth is shown in Figure 8.

The detailed experimental study of the complex pump-probe detuning behavior, especially at high intensities ($1 >> I_{sat}$) is important in demonstrating and understanding the longitudinal mode properties of a PCR employing sodium as a phase conjugating mirror.

C. OPERATION AND DETAILED STUDY OF A cw PCR USING A LARGE BANDWIDTH PCM

The layout for the PCM described in Figure 1 was incorporated into the experimental arrangement shown in Figure 9. This experimental arrangement provides an alternate small-angle "probe path" which is collinear with what essentially amounts to a cw dye laser without its output coupler. The alternate "probe path" thus constitues the optical path of the PCR, with the argon-ion pumped dye jet forming the gain medium, and the Na cell PCM (and the f = 25 cm coupling lens) replacing the

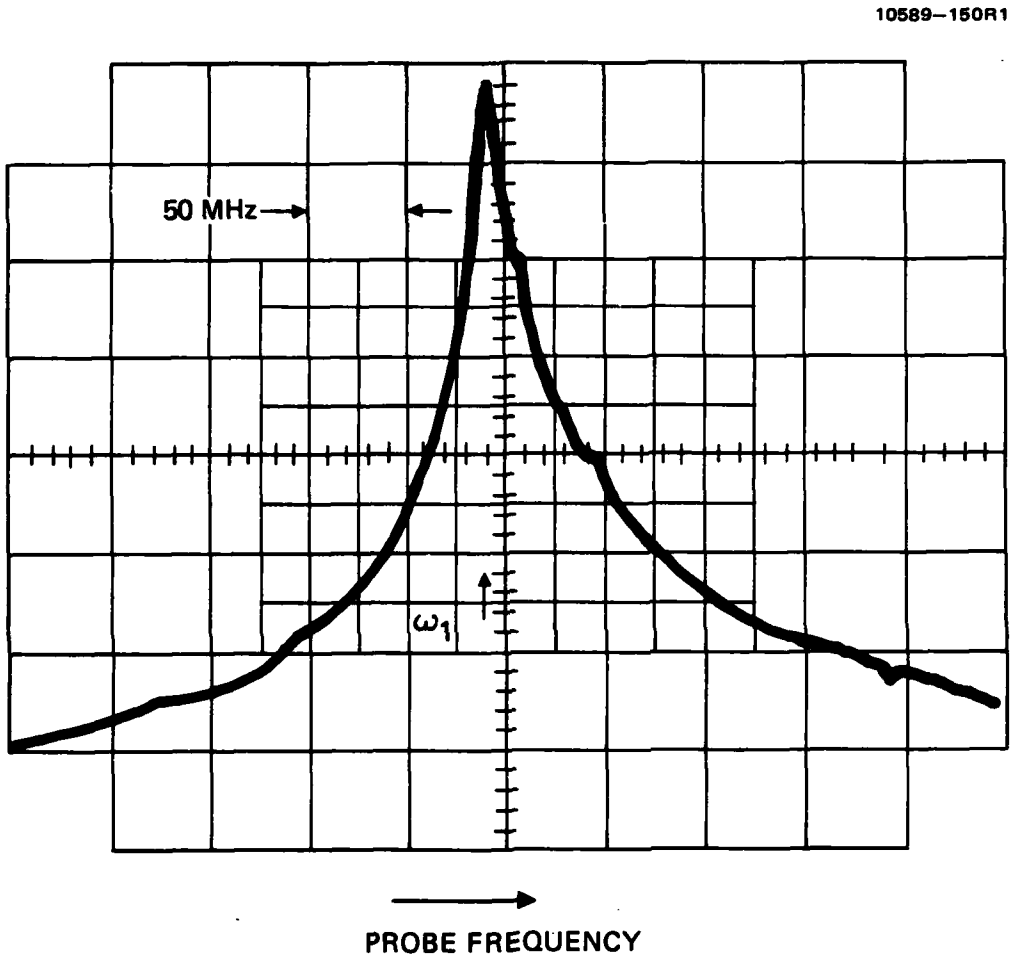

Figure 8. The bandwidth of the pump-probe detuning signal under high reflectivity conditions ($R \approx 150\%$, $\alpha\ell \approx 30$).

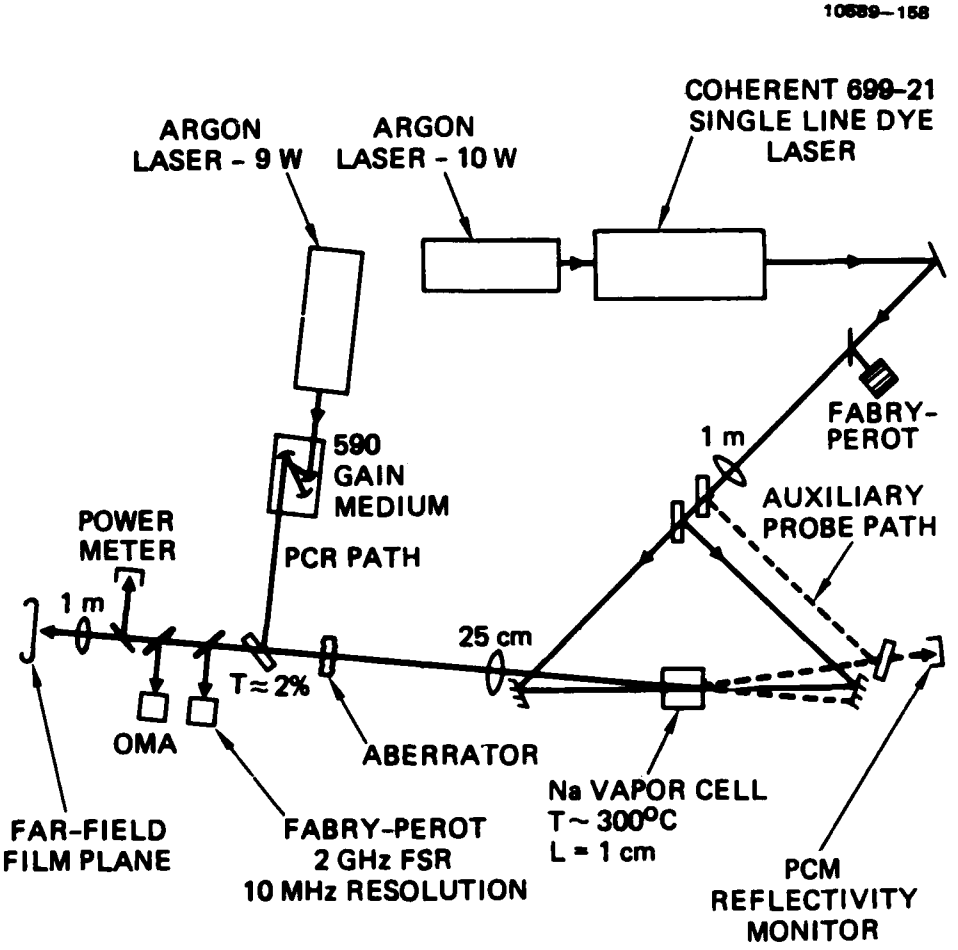

Figure 9. Experimental configuration for a cw PCR. The PCM is produced using DFWM in sodium vapor. The PCR gain medium is an argon pumped dye laser using Rh6G dye.

conventional output coupler. The high reflector end of the standard folded mirror dye laser cavity corresponds essentially to a 100% reflectivity conventional mirror in the standard 2-mirror PCR. Oscillation was easily obtained in such a PCR, and the resonator output was coupled by the T ~ 2% beam-splitter shown in Figure 9. This output was monitored with an optical multichannel analyzer (OMA) and with a 10 MHz-resolution scanning Fabry-Perot etalon. The OMA indicated that the PCR output was at 5890 Å as expected, but when the PCM was replaced by a conventional mirror with relectivity equal to that of the PCM, the laser oscillated near 5840 Å (at the peak of the gain for R6G).

In out experiments two distinct operating modes were observed: pure single longitudinal mode output (without the use of any intracavity frequency selecting elements) as shown in Figure 10(a); and multimode structure consisting of the paired half-axial modes as shown in Figure 10(b), with a frequency separation of c/4L as expected. To understand why these operating modes occur, it is necessary to review the pump-probe detuning characteristics[7] of the nearly-degenerate four-wave mixing that may occur in this PCM. Our earlier observations showed that a high pump intensities, the probe frequency at which the peak reflectivity of the PCM occurs need not coincide with the pump frequency. Furthermore, the bandwidth of the PCM is also a function of the pump detuning from resonance. To determine the effects of the PCM bandwidth on the PCR output, we compare this bandwidth to the c/4L spacing of the PCR. In these experiments c/4L ~ 40 MHz; thus, the first set of paired half-axial modes will occur with a total separation of 80 MHz. We also noted in our PCR experiments that when the pump frequency was adjusted so that the peak reflectivity of the PCM occurred for a probe frequency equal to the pump frequency, the PCR oscillated in a single longitudinal mode (Figure 10(a)). From the independent bandwidth measurements under these conditions (see Figure 6) it was found that the FWHM of the PCM filter was

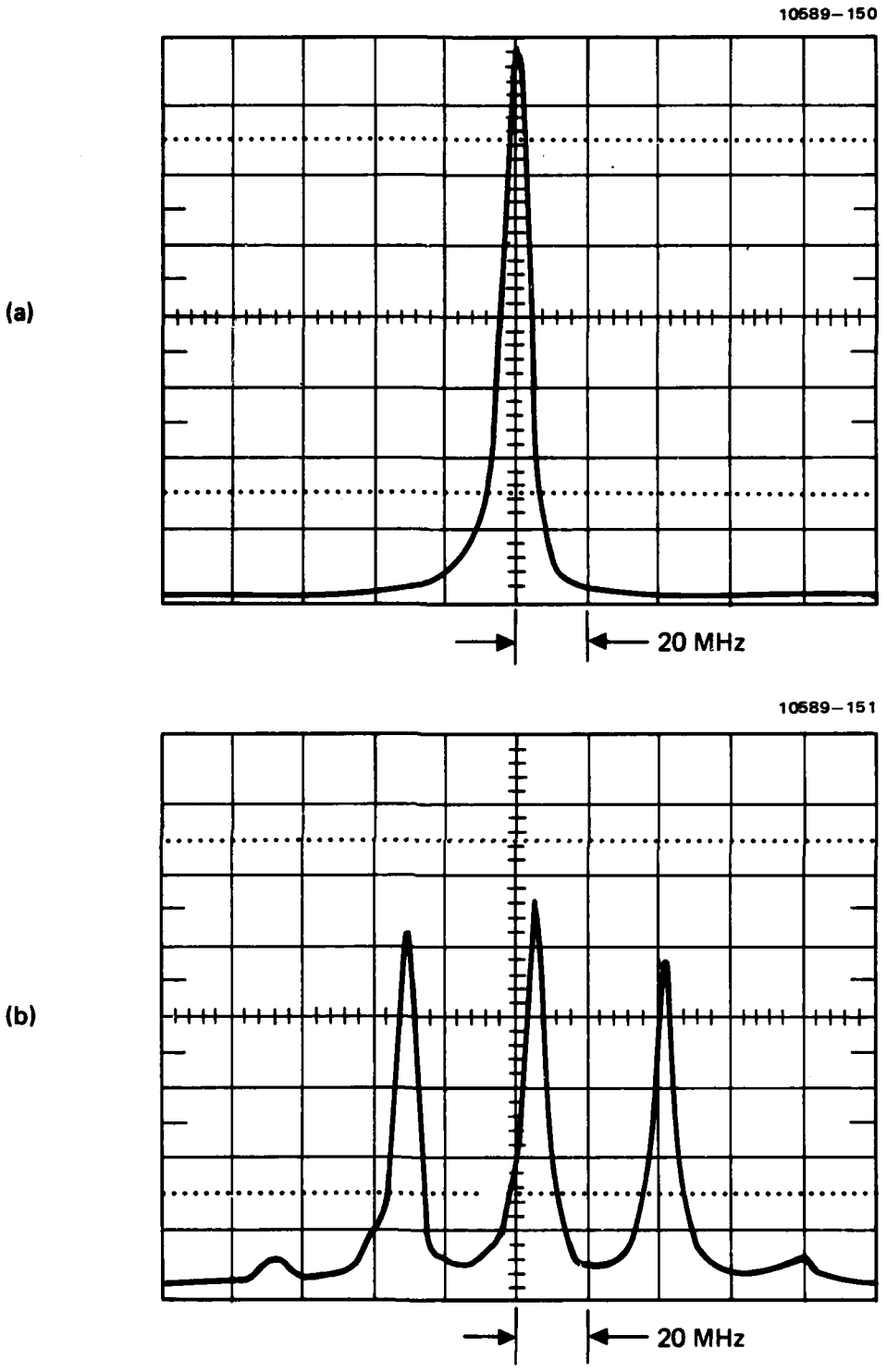

Figure 10. Scanning Fabry-Perot signals of PCR output. Figure 10(a) shows single mode output when the PCM bandwidth is less than c/4L. Figure 10(b) shows the paired half-axial modes separated by c/4L when the PCM bandwidth is of order 200 MHz.

about 50 MHz consistent with suppressing the modes that would oscillate at a separation of 80 MHz. However, when the pump frequency was repositioned so that the PCM bandwidth opened up to $\gtrsim$200 Mhz, the PCR was observed to oscillate in several paired modes (consistent with the increased bandwidth), centered around the pump frequency, w_1, as in Figure 10(b).

The peak output power observed from the PCR was measured and found to be about 1 mW. This is consistent with a calculation that takes into account the unique saturation characteristics of a PCR. In particular, in a conventional dye laser the saturation of the system is determined by the saturation intensity of the dye gain medium, which is on the order of ~1 MW/cm^2. However, for a PCR oscillating with the geometry shown in Figure 9, the saturation characteristics are determined by the PCM; i.e., the maximum internal flux in the PCR can be no greater than the pump intensity used for the PCM. Thus, the saturation intensity of the PCR is determined by the pump intensity of the PCM, which in this case is about 50 W/cm^2. If one assumes that the reflectivity of the conjugator saturates as $1/(1+I/I_{sc})$, it is easy to show that the output power (assuming mirror losses are negligible) is

$$P_0 = (AI_{sc}) \frac{(1 - R_1)}{R_1 G_0} \left(R_1 R_{PCM} G_0^2 - 1 \right) , \qquad (1)$$

where $G_0 = e^{g_o L}$, I_{sc} is the conjugator saturation intensity, A is the area of a resonator mode, and R_1 and R_{PCM} are the reflectivities of the conventional and PC mirrors respectively. We inferred G_0 from measurements made when the PCM was replaced by an ordinary mirror (using standard expressions for output power from dye lasers). Our measured values were within an order of magnitude of those calculated from Equation (1).

The transverse mode properties of the resonator have not been analyzed fully yet; however, the output beam occurs in the

form of a bright spot similar to the TEM_{oo} mode. Qualitative features of the transverse mode properties have been analyzed by observing the aberration correction ability of the PCR in the presence of a fixed intracavity aberrator. (Use of the high-speed real-time correction capability corresponding to the PCM bandwidth of ~100 MHz will be subject of future work.) The fixed aberrator used corresponded to ~10 times the diffraction-limited spot in the far field and was positioned in a manner so that it was completely imaged by the 25 cm lens (see Figure 9) into the interaction volume of the PCM. Figure 11 shows the aberration correction ability of the PCR. Figure 11(a) and 11(b) show the PCR output through the 2% output coupler, both without and with the aberrator, thus showing aberration correction. Figure 11(c) and 11(d) show the PCR beam that is transmitted through the PCM, without and with the aberrator, demonstrating, as expected, that no aberration correction is obtained on the beam transmitted through the PCM. The aberrator is only single-passed when observing the beam at this position (see Figure 9, dashed line). Also, when the PCM was replaced with a conventional mirror of comparable reflectivity, no lasing action was observed until the aberrator was removed, illustrating dramatically, albeit qualitatively, the ability of the intracavity conjugation process to compensate for unusual diffraction losses within the PCR. The real-time correction ability of the large bandwidth PCM was also demonstrated qualitatively by noting that the output of the PCR was relatively insensitive to movements of the aberrator at nominal "hand-held" speeds.

D. SPATIAL AND TEMPORAL PROPERTIES OF A cw PHASE-CONJUGATE RESONATOR BASED ON PHOTOREFRACTIVE $BaTiO_3$

Phase-conjugate mirrors based on degenerate four-wave mixing have been used to demonstrate the operation of cw phase-conjugate resonators, and to study their longitudinal modes and aberration correction properties.[7,13,14] Of particular interest

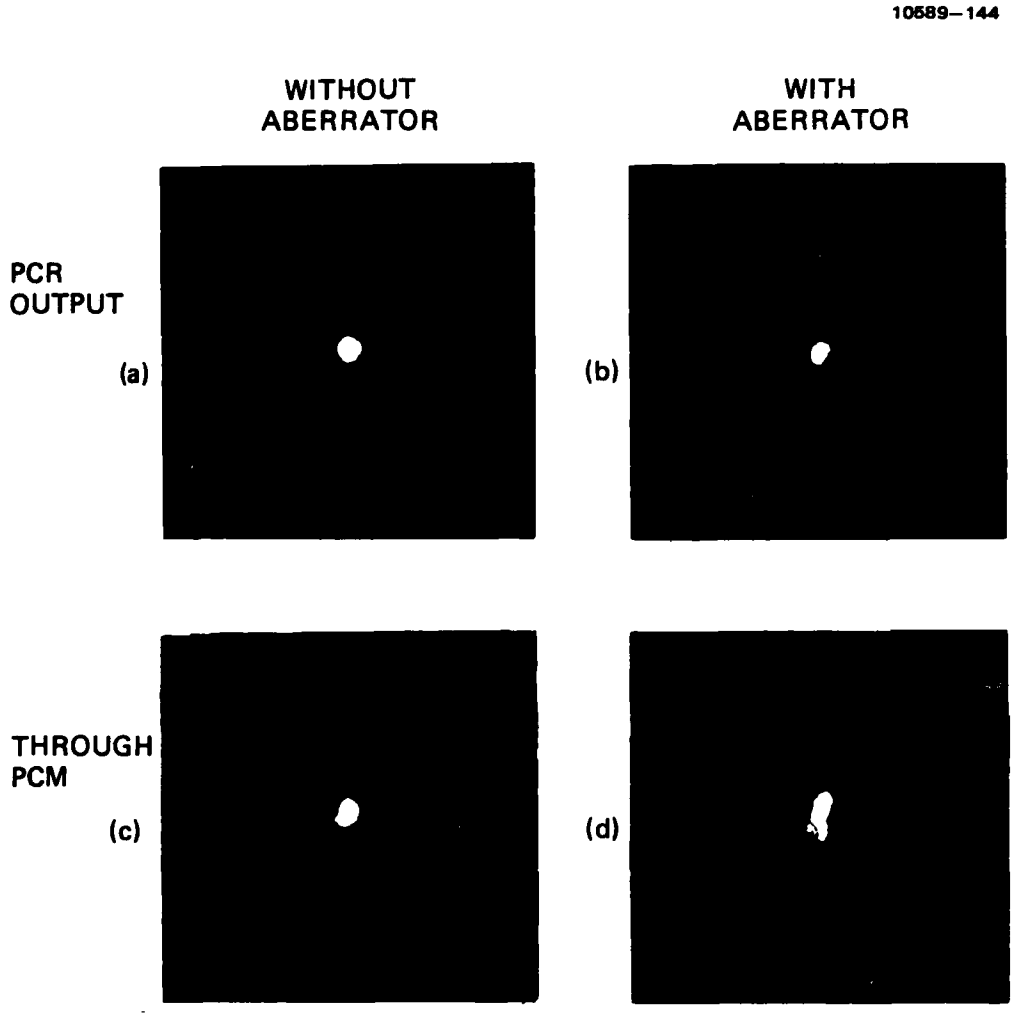

Figure 11. Far-field photographs showing the aberration correction ability of the PCR. Figure 11(a) and 11(b) shows the correction ability of the PCR output in the presence of an aberrator. Figures 11(c) and 11(d) shows the output with the aberrator as observed through the PCM. As expected, Figure 11(d) shows no correction while Figure 11(b) shows good correction.

for this application are the extremely high cw reflectivities[13] that are obtainable from phase conjugate mirrors based on photorefractive crystals such as barium titanate and barium strontium niobate,[15,16] even with the use of relatively low pump powers. These high reflectivities are directly attributable to the magnitude of the photorefractive effect in these crystals caused by the anomalously large values of appropriate electro-optic coefficients (r_{42} = 820 x 10^{-12} mV^{-1} in $BaTiO_3$). It is well known[15-18] that the anisotropy of these electro-optic coefficients (r_{13} = 8 x 10^{-12} mV^{-1}, and r_{33} = 23 x 10^{-12} mV^{-1} for $BaTiO_3$) also cause large asymmetric self-defocusing of beams propagating through these crystals. We have demonstrated experimentally the consequences of this intracavity self-defocusing on the transverse modes of a $BaTiO_3$-based phase conjugate resonator (PCR) when no intracavity apertures are used. The effect of severe intracavity phase aberrators on the transverse mode profile was also studied. In addition, we report data on typical buildup times for steady state oscillation in such resonators, for cases when the coherence length of the pump radiation is either much larger than or much smaller than the round trip distance in the phase conjugate resonator.

Figure 12 shows the experimental arrangement used for our degenerate four-wave mixing (DFWM) and PCR studies. BS1, BS2, and BS3 are 2%R, 18%R, and 66% beamsplitters, respectively, used to generate the three input waves for the DFWM experiments. These are designated by p, f, and b corresponding to the probe, forward pump and backward pump waves in the usual DFWM nomenclature,[7] which correspond to the image, reference, and readout beams in the nomenclature of holography.[13] We will designate the corresponding beam powers and intensities by P_i and I_i, respectively where i = p, f, or b. ND represents variable neutral density filters that were used to attentuate the probe beam, and BB, M3, Ab, and L2 represent a beam blocker, partially transmitting mirror, aberrator and 5-cm focal length

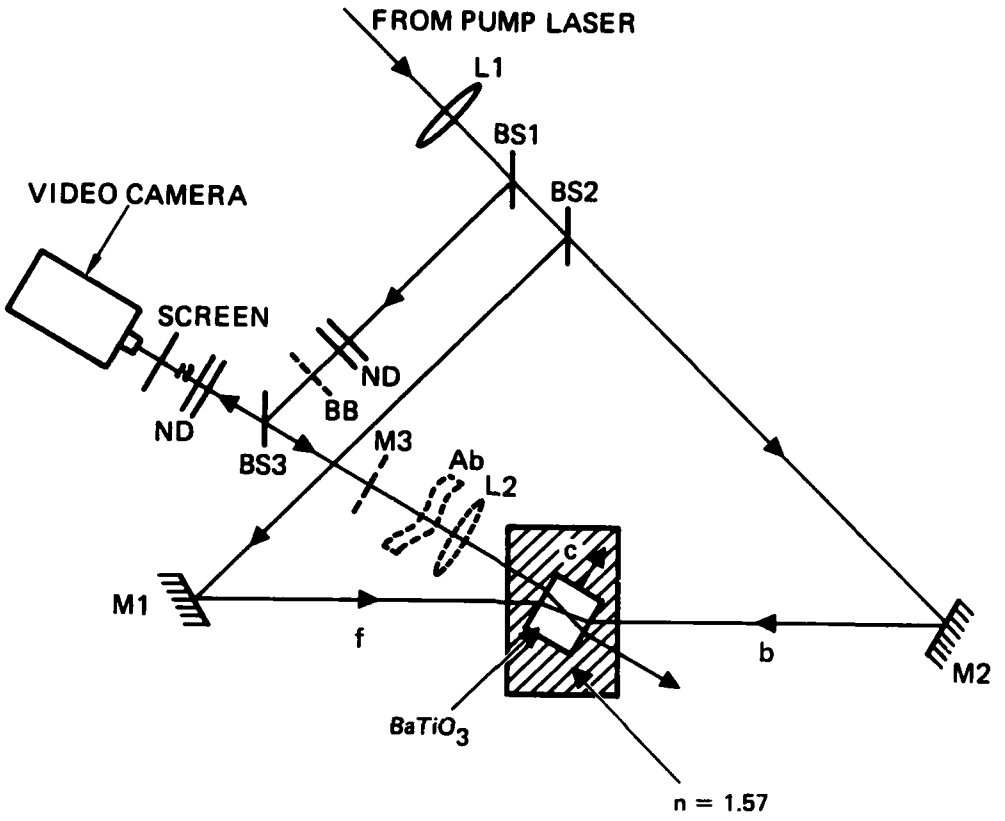

Figure 12. Schematic of the basic experimental layout. The dashed lines represent optical elements that are inserted only for some of the experiments (see text).

lens that were inserted only for PCR studies. The lens, L2, allows focusing of all the light scattered by the aberrator into the pump volume determined by the overlap of the backward and forward pump waves; this not only improves the efficiency of the interaction, but is also essential for proper phase conjugation and aberration correction of this wave. The focal length of lens L1 was 100 cm; the path lengths of all three waves from this lens to the $BaTiO_3$ crystal was 100 cm ± 1 cm; the less than 2 cm path length difference was much smaller than the coherence length, ℓ_c, of any of the lasers used in these experiments.

Experiments were performed using either a 15 mW multilongitudinal mode TEM_{oo} He-Ne laser output at 6328Å (ℓ_c ~20 cm), or using ~100 mW of multilongitudinal mode or single longitudinal mode TEM_{oo} power at 6471Å from a Kr^+ ion laser. A Faraday isolator was inserted between the experimental configuration of Figure 1(a) and the pump laser to avoid instabilities associated with the inevitable retroreflection of beams from the experimental configuration to the pump laser; this isolator was found to be crucial for well-characterized single longitudinal mode pumping of the PCR (and of the DFWM interaction). With multimode operation the data corresponding to both the 6328-Å and 6471-Å experiments was very similar except for the increased speed[13,14] at the higher 6471-Å powers. For the data reported here, all of the beams were p-polarized, and the external angle, θ (see Figure 13), between the probe and forward pump beams was maintained between 20 and 25°. The 5 mm x 5 mm x 5 mm piece of single domain crystal $BaTiO_3$ was poled[19], by us just prior to [20] these experiments and was placed in a high refractive index (1.57) fluid with an angular orientation (see Figure 13) similar to that of Ref. 13.

Using the above configuration, with backward pump-to-forward pump (I_b/I_f) and forward pump-to-probe (I_f/I_p) intensity ratios of between 4 to 1 and 10 to 1, phase conjugate reflectivities of over 200% were observed over a wide range of pump powers (from P_b ~5 mW to ~100 mW; i.e., I_b ~5 W/cm^2 to ~100 W/cm^2) for both single longitudinal mode and mutimode laser operation. For PCR operation, it is critical that the probe beam retraces its path exactly, which imposes a severe constraint on the relative angular alignment of the two pump beams. The angular fidelity of the phase conjugate return was checked with the use of a small variable aperture in the path of the probe beam. To obtain PCR operation, this aperture was removed, the probe beam was blocked (by BB in Figure 12), and a partially transmitting mirror M3 (T = 2% to T = 40%) was oriented perpendicular to the path of the original probe beam.

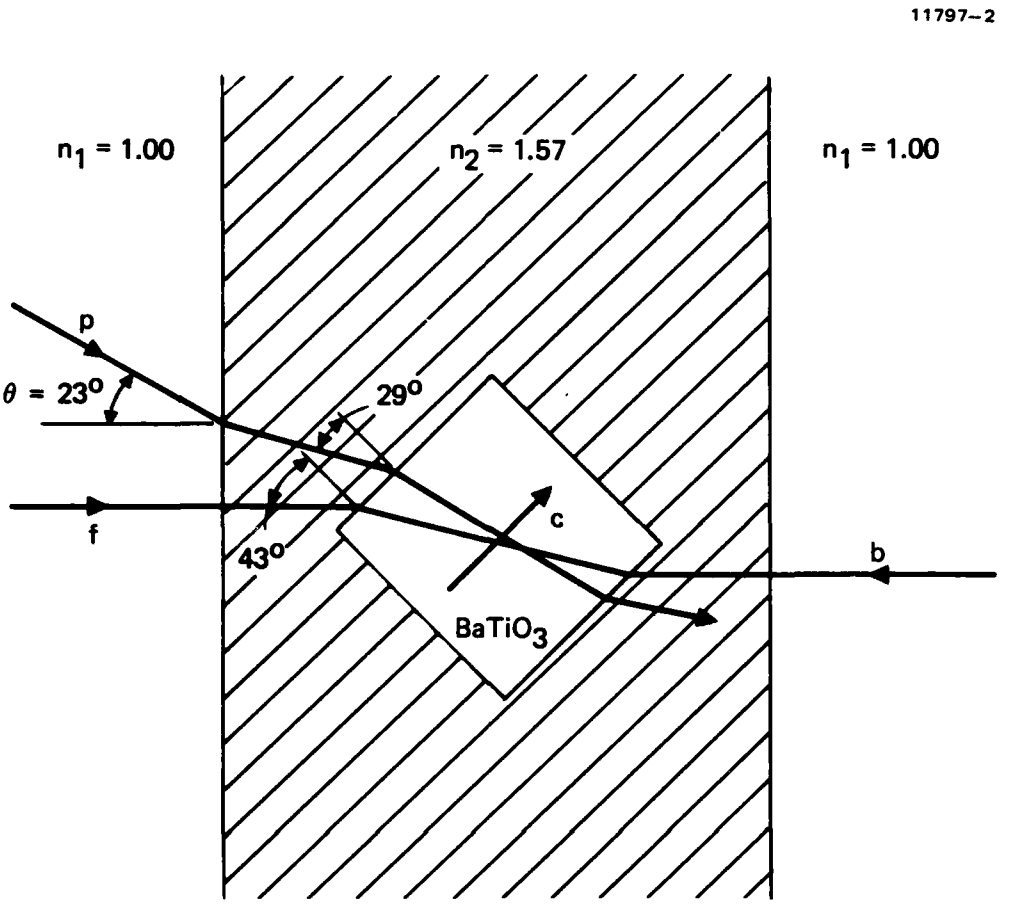

Figure 13. Details of the angular orientation of the $BaTiO_3$ crystals and input beams. The arrow marked c designates the direction and polarity of the crystal axis.

Oscillation of the PCR was then observed to occur with a relatively slow buildup time; we will first discuss the mode structure versus the steady-state oscillation.

Figure 14 depicts far field photographs and transverse mode profiles of the output of such a "$BaTiO_3$ PCR" when pumped by single longitudinal mode TEM_{oo} radiation from a Kr^+ ion laser. All of these photographs were taken in the direction of M3, as indicated by the location of the video camera in Figure 12. For these experiments, P_f = 0.75 mW and P_b = 3.5 mW, and an output

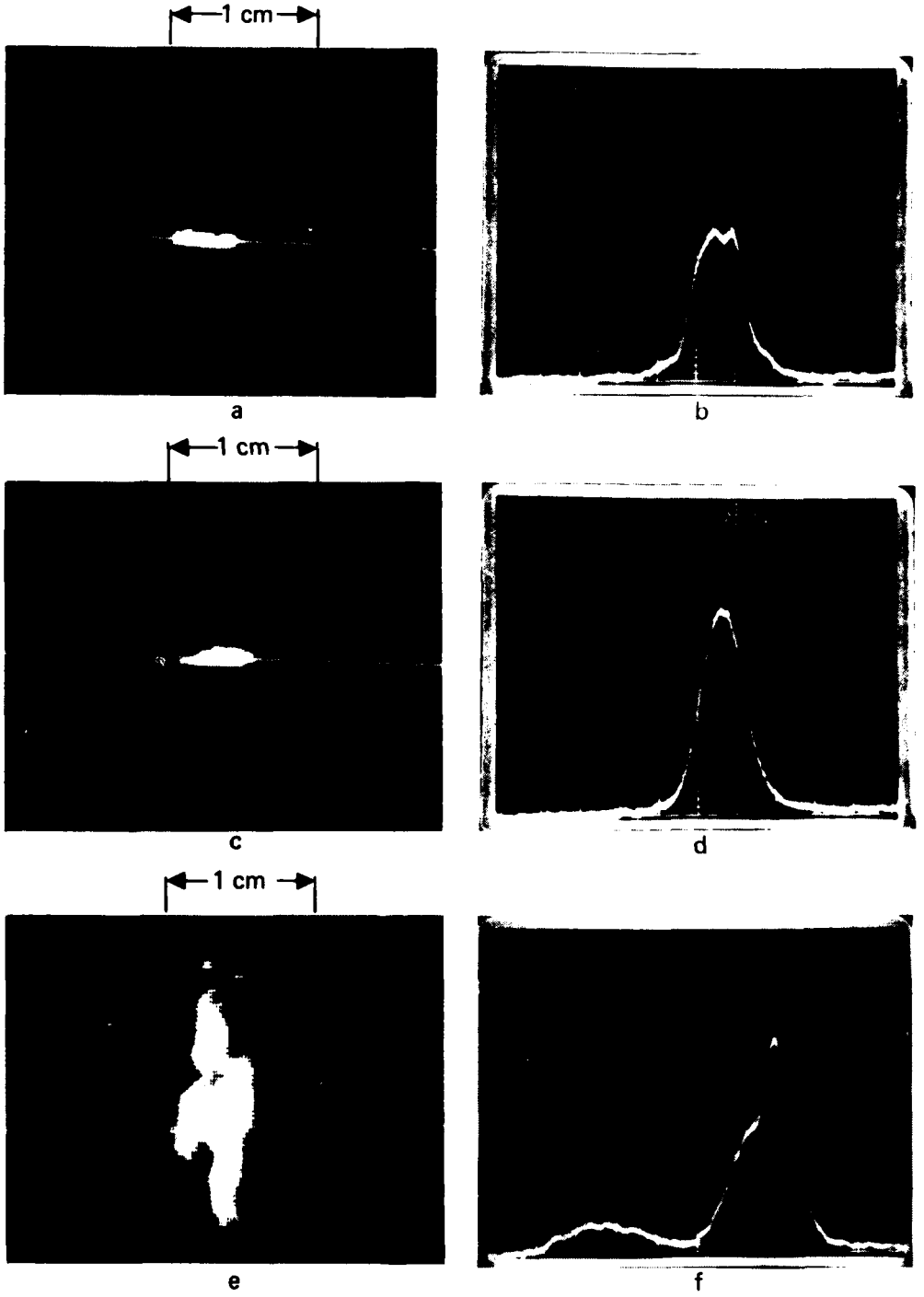

Figure 14. Far-field photographs (a), (c) and (e), and corresponding intensity profiles (b), (d) and (f) of the output beam from the PCR. The intensity profiles correspond to the location of the cursor in the far field photographs. (a), (b): no intracavity aberrator. (c), (d): with intracavity aberrator. (e), (f): characterization of the aberrator.

coupler (M3) with T = 7% was used. Figure 14(a) and 14(b) correspond to the case with no intracavity aperture or aberrator. It is observed that the "natural" transverse modes of such a resonator show a distinct elongation (~4 to 1) in one direction. The elongation is in the plane defined by the input beams and the crystal axis, and is in qualitative agreement with the dominant beam coupling or beam defocusing in this direction due to the anisotropy of the photorefractive effect,[15-18] and the value of the numerical aperture (or acceptance angle) of lens L2. No attempts were made to model such transverse mode behavior theoretically. Aperturing the beam results in a more circular spot, but with significant loss of output power,[21] as expected from spatial selection of the PCR transverse mode from the laterally elongated pump-probe overlap region in $BaTiO_3$.[17,18] The transverse mode profile of Figure 14(b) is along the direction of the horizontal cursor (white line) of Figure 14(a). The homogeneity of the beam profile was also observed to vary slowly with time (on a time scale of several seconds), and the slight dip in the oscilloscope photograph of Figure 14(b) is not a characteristic of the mode structure. Figures 14(c) and 14(d) show far-field photographs of the beam and the transverse mode profile when a severe aberrator is placed inside the cavity. The attenuation of the camera was reduced by an ND of 0.6, indicating a reduction in the beam intensity by approximately a factor of 3 due to the insertion loss of the aberrator. The relatively small change in the overall beam profile is indicative of excellent aberration corretion, and is in strong contrast with the irregular mode patterns in the transverse mode data of Ref. 13. We do not understand the exact reasons for this discrepancy; however, we did observe similar irregular mode patterns when we used multi-longitudinal mode radiation for pumping the PCR. Figures 14(e) and 14(f) characterize the aberrator and were obtained by unblocking the probe beam, blocking the two pumps, and inserting a 100% retroreflector next to the aberrator (between the aberrator and lens L2), so that these

pictures characterize the far-field pattern obtained after double passing the aberrator. Care was taken to ensure that the spatial region of the aberrator that was sampled by the probe beam was identical to the one for which the data of Figure 14(c) and 14(d) were taken. We note that the mode profile of Figure 14(f) shows the shortcomings in the rendition of the intensity profile by merely a single-exposure photographic observation[7,13] (such as Figure 14(e)), due to the lack of linearity of most photographic recording materials.

Additional experiments were performed to confirm that the observed output was indeed a PCR oscillation and not merely due to self-sustained beam coupling effects[22,23] initiated by gratings that may have been written into the crystal at an earlier time. This included observations of the decay and buildup of the PCR oscillation with the blocking of the output coupler, M3, and the observation that the PCR oscillation "tracked" small angular adjustments of this mirror in both the horizontal and the vertical planes. At pump power levels corresponding to a few mW (beam area ~0.1 mm^2; i.e., pump power densities of a few Watts/cm^2), the typical buildup and decay times of the PCR were observed to be of the order of several seconds (~25 sec for I_f - 1.2 W/cm^2, I_b = 5.6 W/cm^2), and were comparable to the measured response times of the $BaTiO_3$ crystal at these power densities.

When the $BaTiO_3$ crystal was pumped with a multi-longitudinal mode laser (He-Ne or Kr^+), such that its coherence length (ℓ_c ~8 cm for Kr^+) was much shorter than the round trip distance (~30 cm) in the PCR, buildup oscillation was still observed to occur in the PCR cavity. However, this oscillation was extremely sluggish, with buildup and decay times that were nearly two orders of magnitude larger than the corresponding values of material response times. Because of the lack of phase coherence between the oscillating beams and the pump beams, it is surprising that any PCR buildup occurs at all, and the observed buildup is perhaps itself a measure of this coherence.

However, as indicated earlier, the observed transverse mode profile was of much more irregular character than that shown in Figure 14. Nevertheless, negligible degradation in the far field mode pattern was observed even when very severe aberrators were introduced into the cavity.

It is conceivable that the coherence constraints imposed for multimode pumping could be satisfied much better if the $BaTiO_3$ crystal were moved one resonator length, L, away in the direction of the backward beam, so that the readout beam, b, arrives at a time, 2L/c, earlier than its precisely coherent counterpart in the reference beam, f. Then, the scatter of the readout beam, b, by the dominant steady-state (f-p) grating would result in a wave that returns after a one round trip (i.e., 2L/c) delay in the PCR as an image beam p that is coherent with f, the other writing beam. A steady state self-consistent solution may thus be possible in which the dominant intracavity flux ("p") in the PCR closely satisfies the requirements of coherence with respect to the forward pump, f. We have not as yet attempted any experiments or the precise modeling of such a PCR configuration.

With the use of high output couplings, net efficiencies of over 25% were easily obtained in the PCR output power relative to the sum of the input powers, despite the large intracavity losses caused by spurious reflections. In the case of large backward pump to forward pump ratios ($I_b/I_f \gtrsim 10$), accounting for reflection losses, we note that over 90% of the power in the backward pump beam was observed to be diffracted in the direction of the PCR output.

E. SELF PUMPED PHASE CONJUGATE LASER OSCILLATOR

The necessity of supplying pump energy in the form of two counterprogating beams from an external laser source to a PCM element is a distinct shortcoming in any practical laser using such a mirror. To derive this energy from the laser itself

employing the PCM is a very desirable objective. Computations by T.R. O'Meara of HRL of the requirements placed on the available gain in the active medium of such laser systems show that high gains are needed. The overall efficiency as defined by the actual useful laser output power tends to be relatively low (typically, 10 to 20%). In addition, complexities associated with the required start-up conditions and procedure could add substantial complications to any system.

During the final year of this program we have operated a laser oscillator in which one reflector is a self-pumped phase-conjugate mirror (PCM). In contrast to previously reported phase conjugate resonator lasers[13] it requires no pumping beams external to the phase conjugator and no mirrors external to the conjugating element. Extensive measurements have been carried out on the spectral characteristics of two embodiments of this oscillator; explicit aberration correction has been verified in a series of far field observations. Initial computer modeling of laser performance using a full three-dimensional propagation code, a saturable gain medium and both a normal and a phase conjugate mirror give results qualitatively in agreement with our measured laser performance. A recent observation of optical gain[24] in directions offset from the input beam of the present configuration suggests that it should be possible to operate several coupled lasers at the same frequency by simultaneously using the same conjugator as a common mirror.

The laser uses a particularly simple self-contained phase conjugating element, as described by Feinberg:[25] a single domain 5 mm x 5 mm x 5 mm crystal of $BaTiO_3$. The operation as a phase conjugator has been ascribed to a four-wave mixing interaction with one edge of the crystal acting as a corner cube retroflector resulting in two counterpropagating pump beams. A cw reflectivity of approximately 30% implies the need of a laser medium of substantial gain to achieve laser oscillation in order to use such a reflector. We have chosen to employ a laser-pumped dye as our gain medium: Rhodamine 6G, pumped by a Q-switched and frequency-doubled YAG laser.

Since this is a pulsed system, there are questions of "start-up" requirements in a laser system using a self-pumped phase conjugate mirror (PCM). If the PCM in such a laser employs a normal $\chi^{(3)}$ process, the reflectivity is proportional to the square of the incident signal. Therefore, no oscillation would start since R = 0 in the absence of oscillation. In the case of $BaTiO_3$, once beam fanning and collapse[25] has occurred to establish a phase conjugate mirror with some reflectivity (R), the reflectivity can persist for long times after the incident beam is removed. The reflectivity remains large even for a subsequent very low power cw incident beam. We first demonstrated this using the output of the doubled YAG laser directly, writing a curved channel in the $BaTiO_3$ with the 1 kHz string of pulses of 185 nsec duration at 532 nm and peak power levels of 100 W. When the Q-switch was disabled, the low power cw second harmonic beam was reflected with comparable reflectivity.

The dye laser configuration used in these experiments is shown in Figure 15. The basic cavity consists of two flat reflectors and a 50 cm focal length lens to provide a stable cavity and a small beam diameter in the dye cell. The gain medium is 2×10^{-4} molar Rhodamine 6G flowing in a 1 cm path length spectrophotometer cell. The cell was tipped aqay from the vertical to avoid the effects of reflection from the cell windows. The pump laser could be focused tightly enough to obtain superfluorescence from the dye but was operated less tightly focused for the experiments being described. The dye laser produced 65 nsec pulses with approximately 460 W peak power, depending upon the repetition rate, when the output was measured from the quartz flat reflector. No beam bending or phase conjugate return was observed in the $BaTiO_3$ crystal without the three prism tuning assembly shown in Figure 15. This was true even for comparable powers in each case. The laser linewidth was approximately 44 Å (4200 GHz) in the nondispersive cavity, narrowing to approximately 1.7 Å (160 GHz) with the

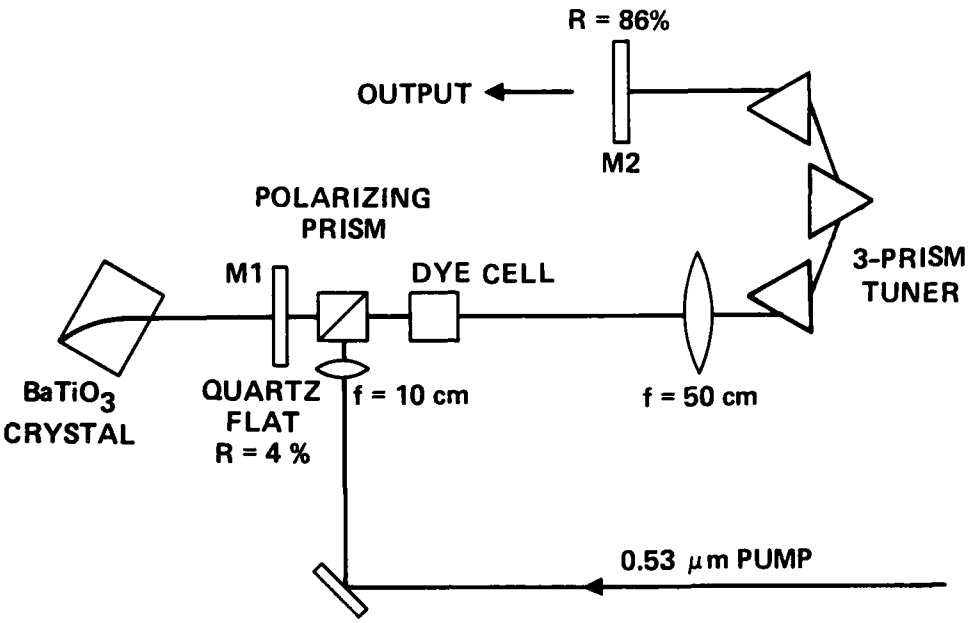

Figure 15. Laser resonator using self-pumped phase conjugator mirror. M1 is removed after writing channel in $BaTiO_3$.

prisms, as measured by a Spex Model 1400 monochromator. Distributed over this overall linewidth were about twelve individual lines whose spacing corresponded to the free spectral range of the quartz flat output mirror (~0.14Å).

The failure to observe the necessary bending of the 44-Å-wide laser beam in the crystal suggests that the bending phenomenon is not simply a consequence of a refractive index wedge, developing as charge migrates from the illuminated region, but requires some degree of monochromaticity for the laser. As the beam initially fans out in the crystal prior to consolidating into a path directed into a corner, a substantial increase in scattered light is observed. A two-beam coupling process in which energy is coupled from the primary beam to a scattered beam directed at an angle to the primary beam is one

mechanism that could be associated with the bending process. Indeed, a requirement for monochromaticity would be operative in this type of coupling.

With the dye laser narrowed by the prism assembly only, the $BaTiO_3$ crystal was placed as shown in Figure 15. As the beam curvature developed in the crystal and the phase conjugator reflectivity was established, an increase in the laser output through the 14% coupler was observed. The quartz flat reflector was removed and laser oscillation continued, with the feedback being supplied entirely by reflection from the crystal. Very little energy remains in the straight-through beam transmitted by the crystal after bending has occurred into the corner and no scattering from this straight-through component was observed inside the crystal. Since this is a pulsed system, oscillation builds up from spontaneous emission as each pulse is initiated. At the operating p.r.f., the grating formed in the crystal tends to degrade only slightly between pulses and is incremented toward some equilibrium condition during each laser pulse. No oscillation takes place without first having written a grating in the crystal with the laser output from the quartz flat reflector. It was possible, however, to observe laser oscillation from such a grating kept in darkness for periods as long as twelve hours, and we believe that even longer periods would be possible for our particular crystal.

A spectral scan of the PCR laser output was made with the Spex Model 1400 spectrometer. Though the laser initially writing the grating was 1.7 Å wide, the measurement showed a PCR laser linewidth of 0.1 Å which was the resolution limit of the spectrometer. To examine this more carefully, a scanning Fabry Perot interferometer was employed; Figure 16(b) shows the spectral structure of the laser output with a total scan of 6.8 Ghz. The half-power bandwidth is approximately 2 GHz or 0.02A, well below what our spectrometer could measure. The fine structure on the trace is real, as seen from Figure 16(b) where the scan width is reduced and spectral structure spaced 181 ±

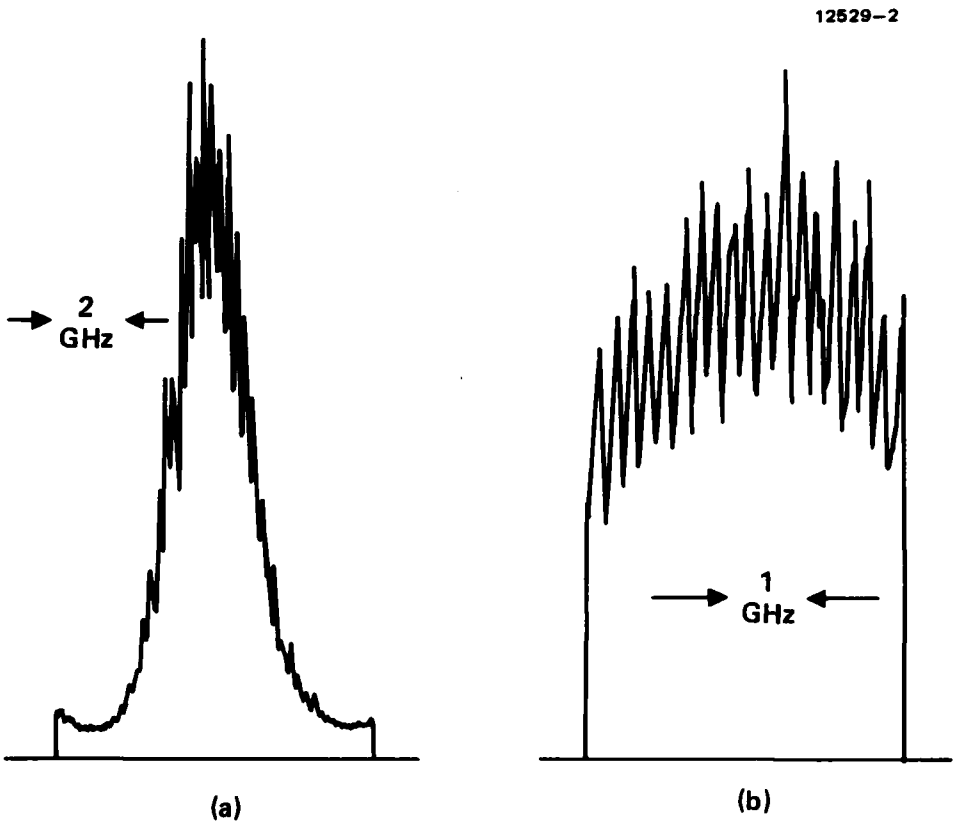

Figure 16. Spectral output of laser. Center wavelength is 5600 Å.

± 8 Mhz is resolved. This corresponds to the usual c/2L axial mode spacing in a conventional resonator, which compares with a calculated 171 + 2 Mhz for our dimensions.[26] This fine structure was not observed on all occasions, for reasons which have not been established.

The operation of the $BaTiO_3$ as the phase conjugating mirror in the laser is shown in Figure 17. In this photograph the beam enters the crystal horizontally near one corner and fans into a very complex array of internal paths. The spectral scan reported above was measured with such a complex structure within the crystal. In general, however, oscillation occurs with only a limited number of tracks, as will be discussed below. The photograph shows the 5 mm cube with the electroded faces and wires used for poling.

Subsequent to our initial observations an attempt was made to remove the electrodes from the crystal using acetone as a solvent. The thermal shock due to rapid solvent evaporation resulted in crystal damage and the formation throughout the crystal of 90° domains which rendered the crystal inoperative for this application. Sanders Associates, the original supplier of the $BaTiO_3$, reworked the crystal by removing the damaged regions and repoling it mechanically. The resulting narrow crystal was successfully operated in the PCR and further measurements were carried out. Figure 18 shows the manner in which the two crystal forms were used.

With the reduced crystal size, very substantial changes were observed in the oscillating linewidth of the laser. At no time was it possible to reproduce the exceptionally narrow linewidth of the earlier crystal. Measurements using an optical multichannel analyser showed that the linewidth depended on the actual path in the crystal and on the point of entry of the laser beam into the crystal. Figure 19 shows three examples where the linewidth was decreased from 13 Å to 2.3 Å by simply translating the crystal normal to the beam and moving the entry point farther along the input face in such a manner that the

13516-4

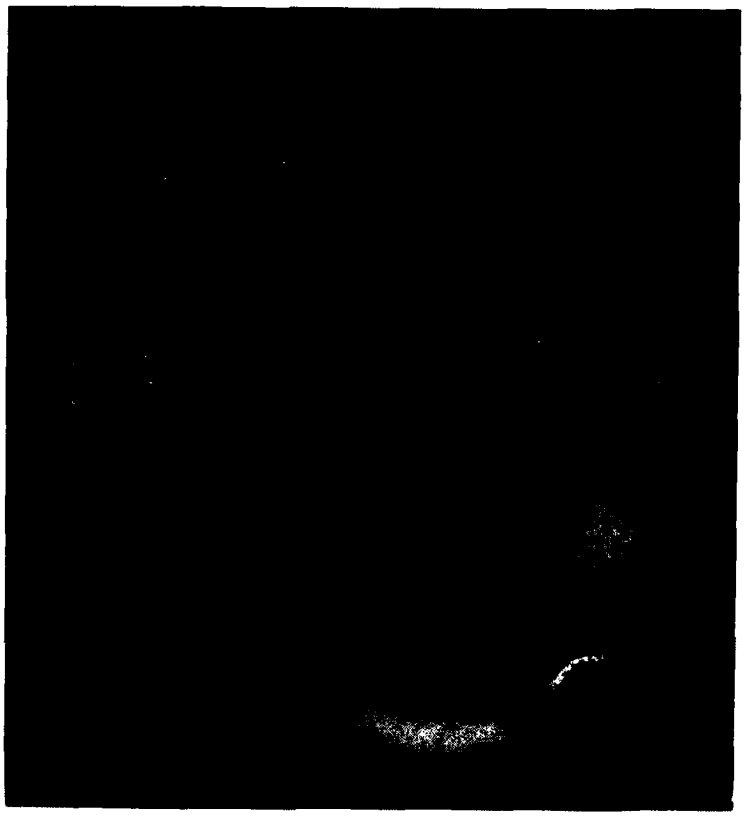

Figure 17. $BaTiO_3$ crystal operating as PCM in laser oscillator.

12970-2

I. CUBE

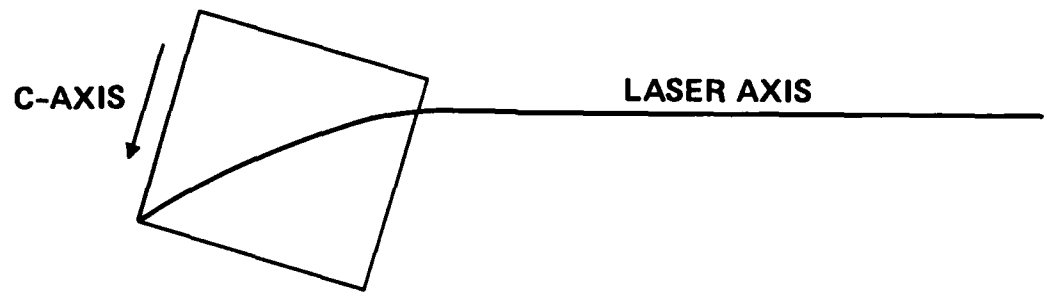

II. NARROW CRYSTAL

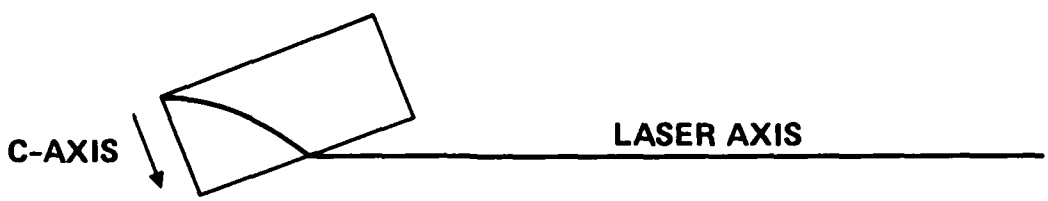

Figure 18. $BaTiO_3$ crystal configurations.

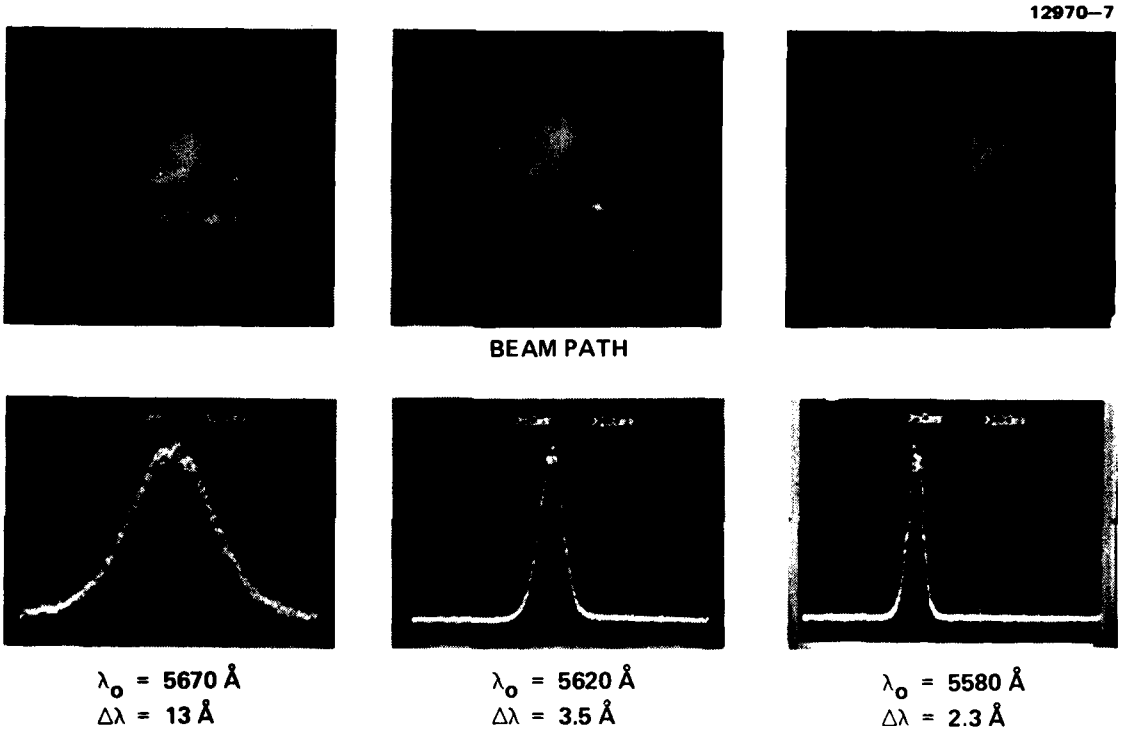

Figure 19. Spectral bandwidth of laser output-narrow crystal.

internal path was increased in length and developed a distinct curvature. The exact mechanism responsible for the narrowing has not been identified. The only correlation with linewidth appears to be the path length within the crystal; additional measurements are required to establish details of its behavior. This is clearly intimately related to the mechanism responsible for the phase conjugating properties of the crystal; at the present time only limited understanding exists of this process itself.

As the crystal was translated beyond the position corresponding to the narrowest linewidth above, a striking breakup of the light path was observed within the crystal. Figure 20 shows that the beam breaks into two pathways, one corresponding to the normal path and the other undergoing total internal reflection at the back surface of the crystal to subsequently bend to the opposite corner. The compound path resulted in the presence of an additional sidelobe in the far field pattern of the laser. No linewidth diagnostics were carried out for this case.

To verify that the $BaTiO_3$ crystal was indeed operating as a phase conjugate reflector, two classes of experiments were carried out. The first of these demonstrates the ability of the conjugator to adapt to the phase front curvatures needed for various mirror positions in the cavity and the second demonstrates the explicit ability to correct for phase aberrations deliberatily introduced into the cavity.

The cavity design, as shown in Figure 15, is such that it is stable for plane mirrors being used at M1 and M2. A movement of more than 2 cm of mirror M1 to increase the cavity length results in an unstable cavity. Using a 100% reflector at M1 and an 86% reflector at M2, output power measurements were made as M1 was moved into the unstable region. Figure 21 shows that a sharp decrease in output power occurred and oscillation stopped completely beyond a certain cavity length. In the unstable region the far-field showed the characteristic ring pattern sidelobe structure characteristic of unstable resonators. The

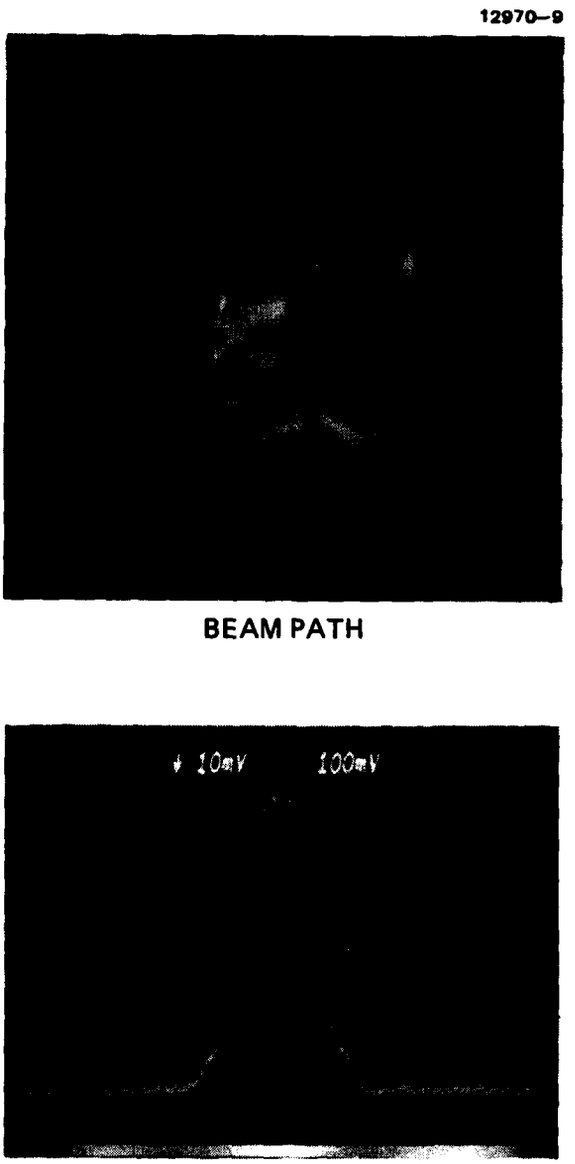

Figure 20. Multiple beam path operation.

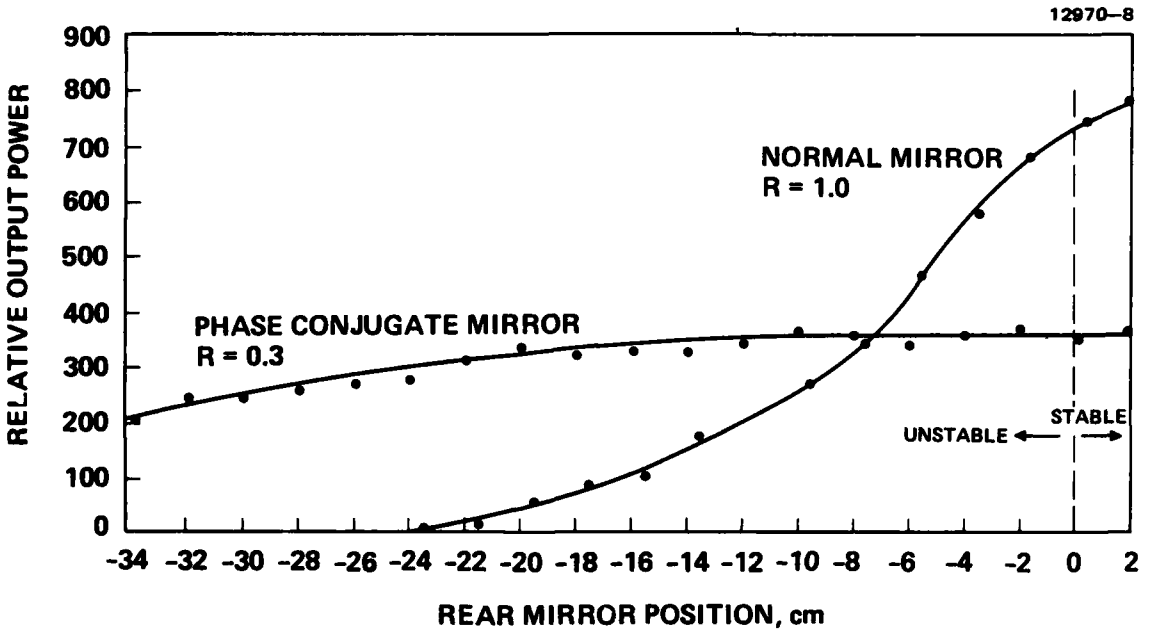

Figure 21. Laser output power dependence on mirror position.

experiment was repeated using the $BaTiO_3$ conjugator reflector. The reflectivity of this reflector was measured to be approximately 30%. As a result, the laser power output was reduced. Note, however, that as the phase conjugate reflector was moved throughout the nominally unstable region, the output power was essentially constant, falling off only slightly at increased cavity lengths. This fall-off is ascribed to the increase in beam cross-section, which can approach or exceed the projected transverse dimensions of the $BaTiO_3$ crystal. The far-field pattern remained a TEM_{oo} mode throughout the entire range of phase conjugate mirror positions.

It is apparent that the phase conjugator is providing the required phase front curvature at the plane of the conjugate mirror to maintain a stable beam configuration within the resonator. There will be a beam waist at some plane between M1ϕ* and M2. This need not have any explicit relationship with respect the the position of the gain medium. But it is expected that the system will be self adjusting to maximize laser output power. With plane normal mirrors at M1 and M2, the beam configuration internal to the resonator is driven to have beam waists both at M1 and at M2. As we will observe below, this difference in internal beam configuration and phase front curvature results in observable differences in the far-field patterns for the two cases.

To examine the far-field intensity distribution, a television camera equipped with level slicing electronics was set-up to observe the beam profile at a distance of 706 cm from M2. The display provides a television picture display format where a given color band represents a signal intensity between two specified levels. In addition, a single line scan provides a direct indication of beam intensity as a function radius. Figure 22 shows the laser output using a plane mirror, R = 100%, at M1. A single horizontal line scan indicates there are small contributions to the output from higher order transverse modes.

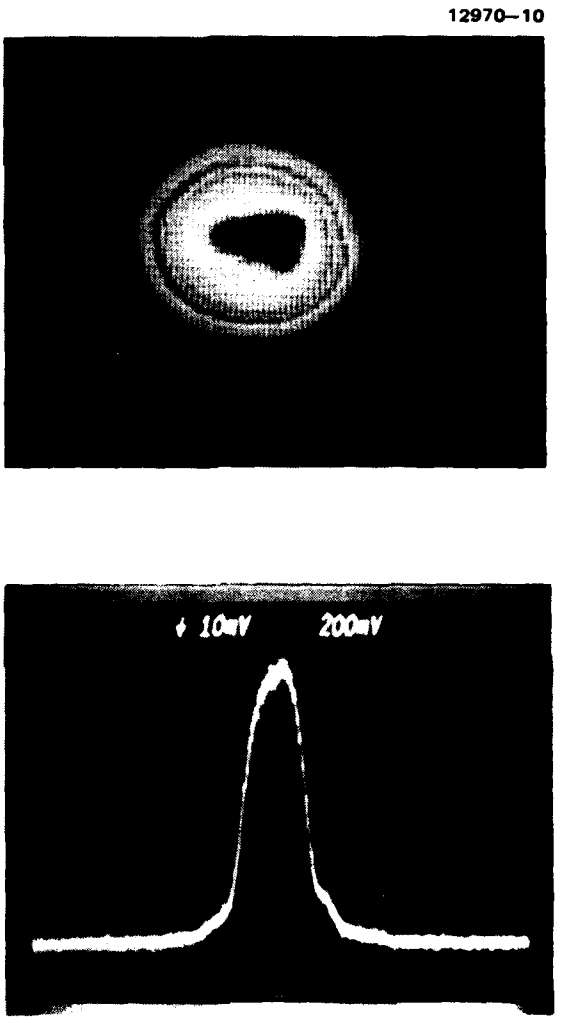

Figure 22. Laser output-far-field-normal mirror.

With the phase conjugate mirror at M1 the output is essentially TEM_{oo} in character with the higher order modes now absent due to a lower reflectivity. Notice that there is a distinct horizontal elongation of the pattern. This is caused by a magnification of the beam in a horizontal plane which originates in the three prism tuner. The beam shows a circular cross-section in the far-field when the laser is operated without the prism tuner. It is apparent that at the observation plane, the PCR resonator beam is somewhat larger than that from the normal resonator. This is due to the different beam profiles and phase front curvatures noted above and will be examined below in our computer modeling. Table 1 summarizes all of the laser operating parameters.

The aberration correcting capabilities of the phase conjugate mirror were demonstrated as follows. Using the 86% relecting output mirror at M2, a 60% reflecting plane mirror was used at M1 and normal laser operation was obtained. A microscope slide which had been distorted by heating with a gas torch was introduced into the cavity between M2 and the prism assembly. At this position the 50 cm f.l. length lens tends to focus any light exiting from the aberrator into the phase conjugator. Except for losses in the dye cell (discussed below) the aberration is essentially one of phase without any associated energy loss.

The aberrator was positioned to produce the far-field pattern shown in the top row of Figure 24. The first panel is a photograph of the beam. Because of the nonlinear response of the film it shows a low level of light and associated structure which surrounds the complex central beam pattern. This main beam has an almost zero intensity on center. The level slicer output and a vertical scan through the pattern are shown in the other two panels.

Without moving the aberrator, the laser beam from M1 (the 60% reflector) was used to write a path in the $BaTiO_3$ crystal. Then the 60% mirror was completely removed, leaving the crystal

Table 1. Laser Parameters

12970-1R1

PUMP LASER	**5320 Å**
$P_{AVERAGE}$	300 mW
PRF	500 pps
τ_P	185 nsec
P_{PEAK}	3.2 kW
DYE LASER	**OUTPUT REFLECTOR 86 %**
$P_{AVERAGE}$ - HR	1 mW
ϕ*	0.46 mW
PRF	500 pps
τ_P	65 nsec
P_{PEAK} - HR	31 W
ϕ*	14 W

WITH R = 4 % OUTPUT MIRROR, PEAK POWER WAS 0.46 kW USING HR REAR MIRROR

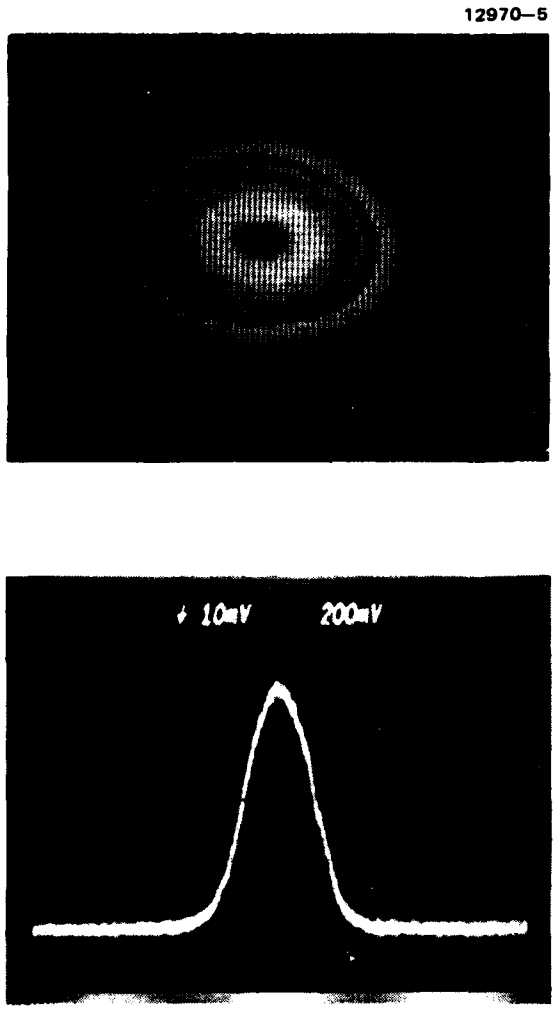

Figure 23. Laser output-far-field-phase conjugate mirror.

alone as the end reflector. With the crystal now functioning as a phase conjugate reflector, laser oscillation continued; the far-field output patterns, are shown in the first panels of the bottom row of Figure 24. A vertical scan through the beam shows an almost perfect TEM_{oo} mode pattern. The phase conjugator has almost totally corrected the internal cavity aberration as far as it affects the output transverse mode pattern. Indeed, an almost TEM_{10} mode is nearly restored to a TEM_{oo} profile. Table 2 summarizes far-field measurements of beam diameter for half-power density.

In terms of output power performance, a comparison with and without the above aberrator also demonstates a substantial, though not perfect, compensation. Examining the ratio of output power, with and without the aberrator, for the case of a normal mirror at M1 and for the phase conjugate mirror at M1, we find for this particular laser:

$$\frac{P100\% + \text{Aberrator}}{P100\%} = 0.19$$

$$\frac{P\phi^* + \text{Aberrator}}{P\phi^*} = 0.55 \quad .$$

Table 2. Summary of Far-Field Measurements at 706 cm From Output Mirror

12970-4R1

LASER CONFIGURATION	MEASURED DIAMETER AT HALF-POWER DENSITY
HR + 86% R	3.0 ±0.2 mm
ϕ^* + 86% R	3.6 ±0.2 mm
ϕ^* + ABERRATOR + 86% R	3.4 ±0.2 mm

Figure 24. Far-field of laser with aberrator in cavity.

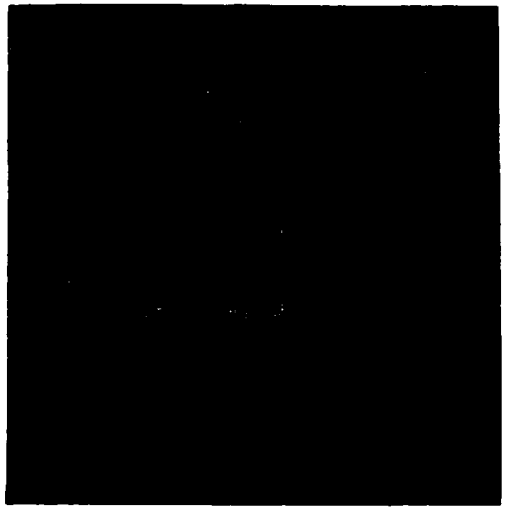

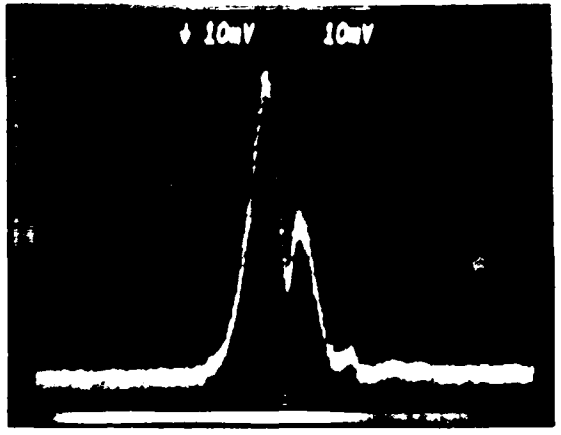

NORMAL MIRROR

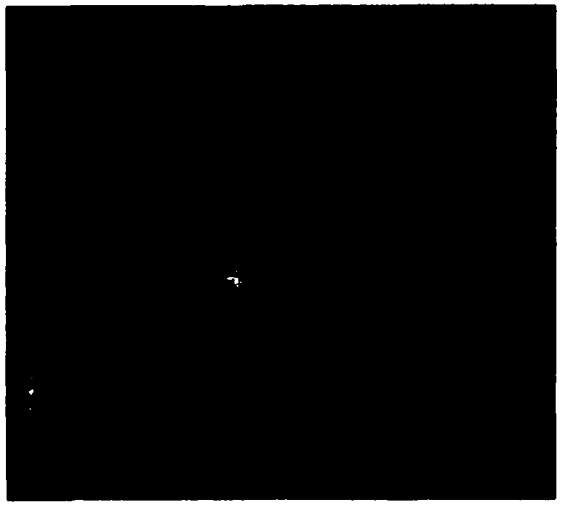

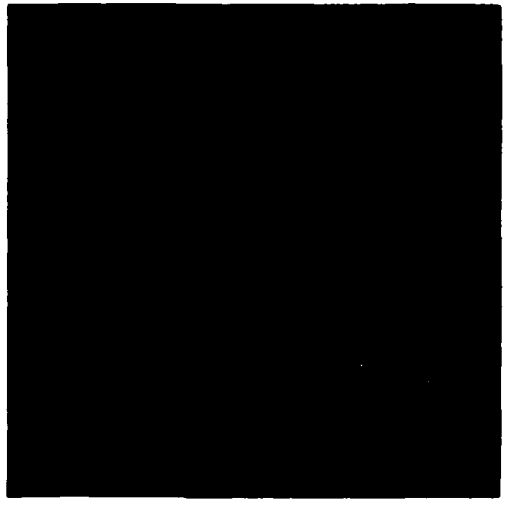

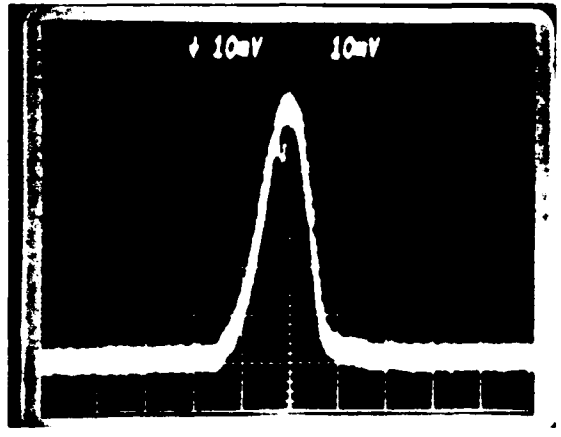

PHASE CONJUGATE MIRROR

We find that not only has the phase conjugate mirror offset the deleterious effects of the aberrator on the transverse mode pattern, but also has rendered the aberration less consequential in determining the output power. The ratio for the resonator employing the phase conjugate mirror should ideally be unity rather than 0.55. As will be seen below, the computer modeling of the present laser shows that in the gain medium there is substantial loss outside the pumped region. Therefore, if the aberrator gives rise to significant deviations of the internal light paths, a reduction in net gain and output power could occur.

Calculations of the properties of the self-pumped phase conjugate resonator were performed with a three-dimensional wave optics computer code developed for a high energy laser by D. Fink (Hughes Aircraft Company, Electro-Optics and Data Systems Division, El Segundo CA). This code has been used previously to investigate phase conjugate resonators and amplifiers.[30-32] The purpose of these calculations was to improve our understanding of energy extraction and transverse mode control in the self-pumped conjugate resonator developed on this program.

The wave optics code provides a three-dimensional, steady state solution to the nonlinear wave equation for the optical field in a convetional or phase conjugate resonator. The field is carried on a two-dimensional grid (typically 128 x 128) and propagated in the third direction by using a fast-Fourier transform to perform the propagation integral in the Huygens-Fresnel approximation. Resonator solutions are obtained by propagating the field back and forth through the resonator until a converged solution (a transverse mode that replicates itself in one round trip) is obtained (Fox and Li method [33]). A wide variety of cw and pulsed gain media models are available in the code, and we have used simple cw saturable gain model,

$$g = \frac{g_o}{1 + I/I_{sat}} \quad ,$$

where g is the gain coefficient, g_o is the small signal gain coefficient, I is the total optical irradiance (as a function of transverse dimensions) and I_{sat} is the saturation intensity. The population relaxation time in the dye gain medium is short compared to the pulse length, so this cw model is a reasonable approximation.[34]

Since a two-dimensional analysis or model of the self-pumped $BaTiO_3$ conjugate was not available, we used a simple model in which the conjugator changes the sign of the phase, reflects the wave and decreases its intensity by a reflection coefficient of 30%, the average reflectivity observed from our conjugator.

A schematic diagram of the resonator as simulated is shown in Figure 25. In previous work we have shown that the transverse mode structure in a phase conjugate resonator is controlled by the smallest internal apertures ot by spatial filters.[31] In the resonator shown in Figure 25 the limiting aperture is the edge of the gain medium, typically about 200 μm in diameter. In our first calculations, we assumed that the region outside the pumped region was completely transparent. This led to output power results that were very different from our observations. In order to check the simulation and to better understand where the discrepancy occurred, we performed a separate calculation using a one-dimensional Rigrod analysis,[35] as described below. Output powers computed from the Rigrod analysis and the three-dimensional code agreed well, and both suggested that large additional losses were present in the resonator which had not been accounted for. Further review of the properties of dye amplifiers[34] suggested that large absorption takes place outside the pumped region of the gain medium. This led us to use a small signal gain with the functional form,

$$g_o = (\gamma + \alpha) \exp(-r^2/r_o^2) - \alpha \quad ,$$

Figure 25. Phase conjugate resonator with optical elements simulated in resonator code. The cross-hatched area of the gain medium is the pumped region. Outside the pumped region the dye acts as a saturable absorber.

where γ is the small signal gain on centerline, α is the absorption coefficient outside the pumped region and r_o is the 1/e point of the small signal gain equal to the 1/e power point of the pump beam). With this model four separate parameters of the dye gain medium are needed: γL, αL, r_o and I_{sat}, where L is the thickness of the dye in the direction of propagation and I_{sat} is abour 10^6 W/cm^2. Since this is the only irradiance value in the calculations, it is simply a scaling factor of the ourput irradiance. The reason one requires only the gain and absorption coefficients times the length is that the thickness of the gain medium is so small that no significant diffraction takes place in the gain medium. Another way of stating this is that the Fresnel number is large compared to unity:

$$F = \frac{k\, r_o^2}{L} >> 1 \quad ,$$

where $k = 2\pi/\lambda = 2\pi/(\text{wavelength})$. For $\lambda = 0.5$ μm, $r_o = 100$ μm, and $L = 1$ mm this yields $F = 126$. The small signal gain was estimated to be $\gamma L \approx 3$. The absorption coefficient was about one-third of this, $\alpha L \approx 1$. The radius of the gain medium was estimated to be 100 μm. Results of the simulations depend sensitively on these values.

There are two measured quantities to which we can compare the code results: total extracted output power from the conventional resonator, and from the conjugate resonator and the far-field beam profiles, as shown in Figures 22 and 23. Table 3 presents the results of the computations where absorption was included outside the pumped region of the dye. As mentioned above, a series of results were obtained with a transparent region outside the pumped dye region, but these appeared to have little correspondence to the observated laser performance.

Comparison of the experimental and theoretical results presented in Table 3 shows several reasonable relationships and a major anomaly that is not understood. First, the computed output powers, while a little high, are in reasonable agreement with the measurements, especially for case 2. Also, the computed powers can be adjusted downward by changing I_{sat}, which could possibly be as low as 5.10^5 W/cm^2. The ratio of conventional power-out to PCR power in the calculations is slightly large, although again, case 2 is in reasonable agreement ($CRP_{out}/PCR_{out} = 3.2$, compared to an observed 2.2) and this agreement could be improved by decreasing the radius, r, of the gain medium. The relative size of the PCR and CR beams in the far-field is also correct. But again, the computed size ratio is somewhat larger than that observed. The ratio of the calculated far-field diameters can be brought into closer agreement with experiment by making the diameter of the gain medium larger, as in care 4. But this causes the powers ratio to disagree more dramatically with observation. We believe that this anomaly is real in the sense that the code calculations are

Table 3. Extracted Power, P_{out}, and Far-Field Half-Power Diameter, D_{np} (at 706 cm) Observed and Calculated with Wave Optics Code for Phase Conjugate Resonator, PCR, and Conventional Resonator, CR.

Experiment				PCR		CR	
				P_{out} 14.2 w	D_{np} 0.36 cm	P_{out} 30.8 w	D_{np} 0.30 cm
Gain Model							
Case	γL	αL	r_o				
1.	3.2	1.2	112 μm	13.0	0.52	94.0	0.25
2.	4.2	1.2	90	17.5	0.56	56.0	0.22
3.	4.2	1.2	100	27.0	0.52	___*	___*
4.	4.2	1.2	112	41.0	0.48	220	0.26
5.	6.0	2.0	140	54.0	0.44	___*	___*
6.	g_oL = 3 r < 130 μm = -1 r > 130 μm			46.0	0.42	320	0.27
* Not Run							

correct simulations of the resonator shown in Figure 25. We suspect that the discrepancy is due to an incomplete physical modeling of either the gain medium or the conjugator. It has been suggested that standing wave effects may be important in the gain medium[36] and that these could easily be simulated with modest modifications of the codes. A more detailed, intensity-dependent model of the $BaTiO_3$ conjugator along the lines of reference 37 could also be implemented in the code. In addition, calculations in which the left-hand mirror is moved away from the gain medium could be performed for comparison with the data of Figure 21.

Rigrod Analysis

Rigrod[35] solved the one-dimensional equations for the propagation of light through a gain medium in a Fabry-Perot resonator, using as variables the forward and backward intensities divided by the saturation intensity, β_+ and $\beta_- = I^{\pm}/I_{sat}$. The equation describing β_+ and β_- is

$$\frac{1}{\beta_\pm}\frac{d\beta_\pm}{dz} = \frac{g_o}{1 + \beta_+ + \beta_-} \quad . \tag{1}$$

Rigrod obtained the outcoupled irradiance, $\beta_{out} = I_{out}/I_{sat}$, for a resonator of the kind shown in Figure 26:

$$\beta_{out} = \frac{T_1 R_2^{1/2} [g_o L + \ln (R_1 R_2)^{1/2}]}{[R_1^{1/2} + R_2^{1/2}] [1 - (R_1 R_2)^{1/2}]} \quad , \tag{2}$$

where T_1 is the transmission coefficient of the outcoupling mirror, R_1 is the total reflectivity of the outcoupling mirror ($R_1 = (1 - T_1)R_{internal}$, where $R_{internal}$ represents internal losses), R_2 is the reflectivity of the right-hand mirror and $g_o L$ is the product of small signal gain times length of gain medium.

We have used Equation (2) to obtain as a function of $g_o L$, values of I_{out} $(R_2 = 1)/I_{out}$ $(R_2 = 0.3)$, which corresponds to the ratio of the laser power-out of our conventional resonator with the perfectly reflecting end mirror, R_2, to our PCR with $R_2 = 0.3$ for three separate values of R_1, as shown in Figure 27. The transmission coefficient of the left-hand mirror is 0.14. Thus, the case $R_1 = 0.86$ corresponds to no additional internal loss ascribed to the outcoupling mirror reflectivity. It is apparent that this cannot give our observed value of $P_{CR}/P_{PCR} \approx 2.2$. If we assume smaller values of R_1, corresponding to a larger internal loss, we can explain our observed power ratio. The origin of this loss in our present system arises from the

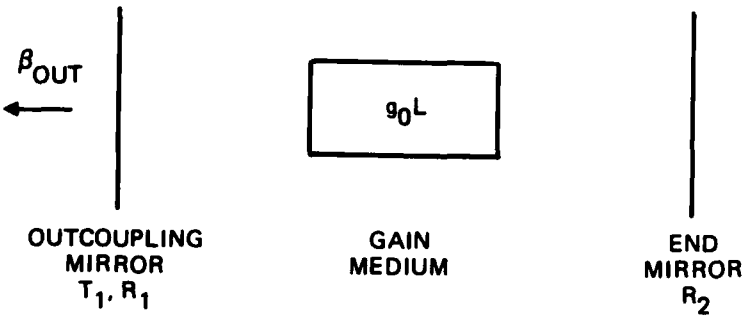

Figure 26. Fabry Perot resonator for Rigrod analysis.

fact that the diameter of the oscillating laser mode at the gain medium exceeds the diameter of gain volume excited by the pump laser. It was this conclusion that led us to modify the gain profile to include a radial profile and attenuation outside the pumped region. The calculated mode profiles exhibit this size relationship.

F. COMMENTS ON SOME OUTSTANDING ISSUES

Since this report represents the first discussion of our observations on self-pumped systems, it will be useful to raise some questions for which additional research is needed. During our experiments on self-pumped $BaTiO_3$ conjugators, damage occured to our original sample. After the crystal was repaired the resulting laser spectral performance, as shown in Figure 19, was dramatically different from that using the full crystal (see Figure 16). The relationship of this behavior to crystal history (i.e., poling electrically or mechanically, etc.) needs to be explored using a number of crystal samples. It is apparent that the oscillator bandwidth is dependent upon the path length of the light in the crystal and the details of the

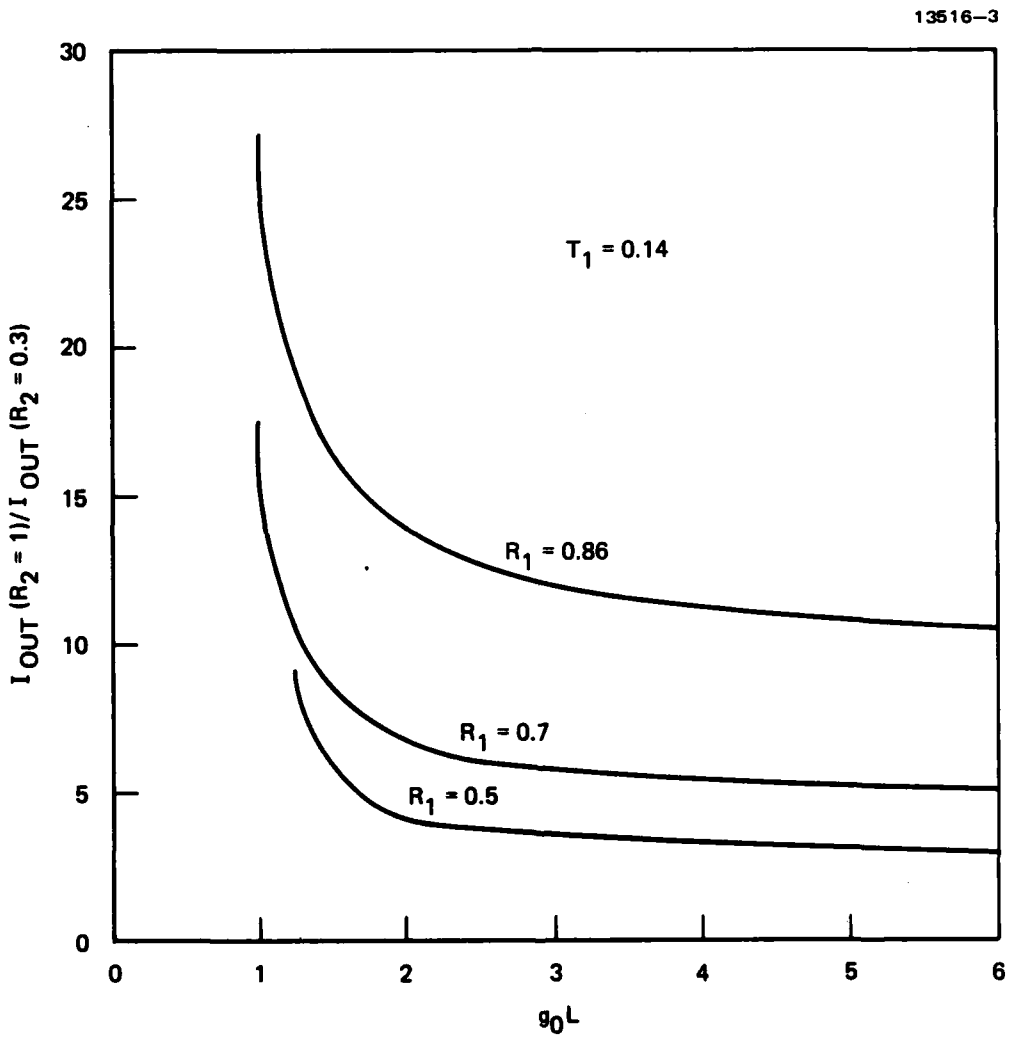

Figure 27. Rigrod results for outcoupled irradiance ratio.

geometry of the laser. Modeling of this behavior should be attempted based upon specific assumed operative mechanisms which give rise to conjugation. Can the theory for the self-pumped conjugator developed by Feinberg be extended to include spectral characteristics? How can we compute the coherence length required for beam bending?

Examination is required of the transverse spatial mode profile of the PCR using real elements. The computer modeling must include the finite aperture of the phase conjugate mirror and the effect of the spatial filter defined by the pumping beam, including the details of a soft or hard aperture behavior. For example, it is clear from the code results reported above that a re-design of the gain region geometry for our present experiments would provide a very substantial increase in output power for the PCR laser. The analysis of the decrease in laser output power for a position of the phase conjugate mirror far into the unstable region of Figure 21, which has been ascribed to a limited transeverse size of the PCM, must consider both crystal boundaries and any variation of reflectivity related to beam intensity variations over the cross-section.

Our experiments have measured a peak reflectivity of the self-pumped PCM of about 30%. Using another crystal sample, measurements on another program at HRL show that a reflectivity of 50% is achievable. A theoretical determination of this parameter is required in terms of material properties and laser intensity. Further, what is the time dependence of the reflectivity in this self-pumped mode and how is it related to the photorefractive response time?

A potentially interesting application of these self-pumped conjugators is suggested by a recent paper by Feinberg.[24] The existance of non-zero reflectivity values for directions offset from the input beam direction in our present laser means that several gain media can be disposed in a plane around a single $BaTiO_3$ crystal. The single crystal can serve as a common mirror

for several laser paths. A coupling between the several laser is provided by one crystal. The configuration should be explored for frequency or phase locking of laser arrays.

Finally, the use of $BaTiO_3$ in the self-pumped mode has so far been limited to a wavelength range of 4500 Å to 6500 Å. The development of new materials or a modification of the optical properties of available materials should be undertaken to extend the self-pumped mode of operation. This could include operation at 8500 Å where applications to diode lasers become possible and at 1.06 μm for use with the Nd:YAG laser. In the latter case, phase distortions due to both thermal lensing and material inhomogenities could be compensated using a PCM.

REFERENCES

1. J. AuYeung, D. Fekete, D.M. Pepper, and A. Yariv, IEEE J. Quantum Electron. 15, 1180 (1979).

2. P.A. Belanger, A. Hardy, and A.E. Siegman, Appl. Opt. 19, 479 (1980).

3. I.M. Bel'dyugin and E.M. Zemskov, Sov. J. Quantum Electron. 10, 764 (1980).

4. J.F. Lam and W.P. Brown, Opt. Lett. 5, 61 (1980).

5. A. Hardy, IEEE J. Quant. Electr. QE-17, 1581 (1981).

6. P.F. Liao, D.M. Bloom, and N.P. Economou, Appl. Phys. Lett. 32, 813 (1978).

7. D.G. Steel and R.C. Lind, Opt. Lett. 6, 554 (1981).

8. J. Nilsen and A. Yariv, J. Opt. Soc. Am. 71, 180 (1980).

9. D.G. Steel and R.C. Lind, Opt. Lett. 6, 587 (1981).

10. J. Nilsen, N.S. Gluck, and A. Yariv, "Narrowband Optical Filter via Phase Conjugation by Nondegenerate Four-Wave Mixing in Sodium Vapor," Opt. Lett. (Aug. 1981).

11. T. Fu and M. Sargent III, Opt. Lett. 4, 366 (1979).

12. D.J. Harter and R.W. Boyd, IEEE J. Quant. Electr. QE-16, 1126 (1980).

13. J. Feinberg and R.W. Hellwarth, Opt. Lett. 5, 519 (1980); erratum: Opt. Lett. 6, 257 (1981).

14. J.O. White, M. Cronin-Golomb, B. Fischer, and A. Yariv, Appl. Phys. Lett. 40, 450 (1982).

15. V.V. Voronov, I.R. Dorosh, Yu. S. Kuzminov, and N.V. Tkachenko, Sov. J. Quant. Electron. 10, 1346 (1980).

16. I.R. Dorosh, Yu. S. Kuzminov, N.M. Polozkhov, A.M. Prokhorov, V.V. Osiko, N.V. Tkachenko, V.V. Voronov, and D. Kh. Nurligareev, Phys. Stat. Sol. (a) 65, 513 (1981).

17. J. Feinberg, J. Opt. Soc. Am. 72, 46 (1982).

18. Our own observations, unpublished.

19. Electric fields of ~1.11 kV/mm were applied for a few hours at a temperature ~145°C (~15°C above the Curie temperature); details of this technique were kindly provided to us by R. Buchanan, Univ. of Illinois.

20. I. Camlibel, M. DiDomenico, Jr., and S.H. Wemple, J. Phys. Chem. Solids 31, 1417 (1970).

21. This varies typically from 30 to 90%, depending on the size of the aperture; similar beam elongation and power reduction with the use of intracavity apertures has also recently been observed by P. Günter, private communication.

22. V.L. Vinetskii, N.V. Kukhtarev, S.G. Odoulov, and M.S. Soskin, Sov. Phys. Uspekhi 22, 742 (1979).

23. B. Fischer, M. Cronin-Golomb, J.O. White, and A. Yariv, Opt. Lett. 6, 519 (1981).

24. J. Feinberg, Opt. Lett. 8, 400 (1983).

25. J. Feinberg, Opt. Lett 7, 486, 1982.

26. The mode structure of a phase conjugate resonator is typically quite different from that of a conventional optical resonator.[27] In a PCR with a PCM externally pumped at frequency ω, the frequency of the principal mode is independent of cavity length, L, and degenerate with the pump frequency, ω. Nondegenerate modes occur in pairs symmetrically spaced about ω.[7] The spacing of consecutive modes on either side of ω is given by c/4L. The phases of the pump waves are assumed to be constant and independent of L for an external pump source.

    In a self-pumped PCR, the phase of the pump beams in the PCM must be included.[28,29] For a PCM with a $\chi^{(3)}$ nonlinearity, it can be shown that if the optical path of the two pump beams is given by ℓ' and ℓ'', respectively, then the output of the PCR has principal modes separated in frequency by $c/(\ell'+\ell'')$ or $c/2\ell'$ for $\ell' \simeq \ell''$, as was observed.

27. A.E. Siegman, P.A. Belanger, and A. Hardy, "Optical Resonator Using Phase Conjugate Mirrors," in Optical Phase Conjugation, R.E. Fisher, ed. (Academic Press, 1983).

28. T.R. O'Meara, private communication.

29. M. Cronin-Golomb, B. Fischer, J. Nilsen, J.O. White, and A. Yariv, Appl. Phys. Lett. 41, 219, 1982 .

30. T.R. O'Meara and G.C. Valley, "Optical Phase Conjugation Applications Study," Air Force Weapons Lab. Technical Report AFWL-TR-82-94 (Jan. 1983).

31. G.C. Valley and D. Fink, J. Opt. Soc. Am. 73, 572 (1983).

32. R.C. Lind, G.J. Dunning, T.R. O'Meara, and G.C. Valley, "Adaptive Pointing Investigation," Air Force Wright Aeronautical Laboratories, AFWAL-TR-83-1016 (Feb. 1983).

33. A.G. Fox and T. Li, Bell Syst. Tech. J. 40, 253-488 (1961).

34. T.F. Johnston, Jr., R.H. Brady, and W. Proffitt, Appl. Optics 21, 2307 (1982).

35. W.W. Rigrod, J. Appl. Phys. 36, 2487 (1965).

36. J.F. Lam, private communication, 1983.

37. K.R. MacDonald and J. Feiberg, J. Opt. Soc. Am. 73 (1983).

PAPERS AND PRESENTATIONS

1. R.C. Lind and D.G. Steel, "Demonstration of the longitudinal modes and aberration correction properties of a cw dye laser with a phase conjugate mirror," Opt. Lett. 6, 554 (1981).

2. D.G. Steel and R.C. Lind, "Multiresonant behavior in nearly degenerate four-wave mixing--the A.C. Stark effect," Opt. Lett. 6, 587 (1981).

3. R.K. Jain and G.J. Dunning, "Spatial and temporal properties of a continuous wave phase conjugate resonator based on the photorefractive crystal $BaTiO_3$," Opt. Lett. 7, 420 (1982).

4. R.A. McFarlane and D.G. Steel, "Laser oscillator using resonator with self-pumped phase conjugate mirror," Opt. Lett. 8, 208 (1983).

5. R.C. Lind and D.G. Steel, "Demonstration of the longitudinal modes and aberration correction properties of a cw dye with a phase conjugate mirror," presented at the Conference on Lasers and Electro-Optics, Washington, D.C., June 1981.

6. R.C. Lind and D.G. Steel, "Demonstration of a phase conjugate resonator," presented at the Gordon Research Conference on Nonlinear Optics, Wolfeboro, NH, Aug. 1981.

7. R.A. McFarlane, J.F. Lam, R.C. Lind and D.G. Steel, "Effects of atomic coherence in resonant degenerate four-wave mixing," presented at the Optical Society of America Annual Meeting, Kissimmee, Fl, Nov. 1981.

8. R.A. McFarlane and D.G. Steel, "Laser oscillator using resonator with self-pumped phase conjugate mirror," presented at the Conference on Lasers and Electro-Optics, Baltimore, MD, May 1983.

9. G.C. Valley, G.J. Dunning, R.K. Jain, M.B. Klein, J.F. Lam, R.C. Lind, R.A. McFarlane, D.G. Steel, K. Stenersen, "Properties and applications of phase conjugate mirrors in $BaTiO_3$," presented at the Gordon Research Conference on Nonlinear Optics, Wolfeboro, NH, Aug. 1983.

END

FILMED

1-84

DTIC